Journal of Computational Physics 435 (2021) 110264

Contents lists available at ScienceDirect

Journal of Computational Physics

www.elsevier.com/locate/jcp

First-passage problem for stochastic differential equations with combined parametric Gaussian and Lévy white noises via path integral method

Wanrong Zan [a], Yong Xu [a,b,*], Ralf Metzler [c], Jürgen Kurths [d,e,f]

[a] School of Mathematics and Statistics, Northwestern Polytechnical University, Xi'an 710072, China
[b] MIIT key Laboratory of Dynamics and Control of Complex Systems, Northwestern Polytechnical University, Xi'an 710072, China
[c] Institute for Physics and Astronomy, University of Potsdam, 14476 Potsdam, Germany
[d] Potsdam Institute for Climate Impact Research, 14412 Potsdam, Germany
[e] Department of Physics, Humboldt University of Berlin, 12489 Berlin, Germany
[f] Saratov State University, 410012 Saratov, Russia

ARTICLE INFO

Article history:
Available online 4 March 2021

Keywords:
First-passage problem
Stochastic differential equation
Fractional Fokker-Planck-Kolmogorov equation
Path integral method
Monte Carlo simulation
Combined parametric Gaussian and Lévy white noises

ABSTRACT

We study the first-passage problem for a process governed by a stochastic differential equation (SDE) driven simultaneously by both parametric Gaussian and Lévy white noises. We extend the path integral (PI) method to solve the SDE with this combined noise input and the corresponding fractional Fokker-Planck-Kolmogorov equations. Then, the PI solutions are modified to analyze the first-passage problem. Finally, numerical examples based on Monte Carlo simulations verify the extension of the PI method and the modification of the PI solutions. The detailed effects of the system parameters on the first-passage problem are analyzed.

1. Introduction

The first-passage problem describes the instant in time when the dynamic variable of a system crosses a preset value for the first time in a given time interval. This problem widely appears in engineering, physical, chemical, and biological systems [1–5]. Typical examples include integrate-and-fire neuron dynamics, in which a neuron fires once a fluctuating voltage level first reaches a specified level [6]; ship roll motion, in which the ship capsizes once the ship roll angle first exceeds the safe range [7]; shallow curved structures (such as arches and shells), whose structure may be destroyed once a snap-through buckling occurs [8]; or financial mathematics, for instance, the stock price level at which a given stock is sold [9]. Prototypical examples also include chemical reactions [10,11] and molecular signaling processes in biological cells [12,13]. First-passage dynamics is often characterized in terms of (global) mean first passage times [2,14,15]. Recent studies show that even in simple geometries repeated first-passage events are vastly dissimilar [16,17] and that the associated spectra of first-passage times [18,19] and reaction-times [20,21] are characterized by time scales spanning several orders of magnitude.

While the above examples are based on continuous random walk processes or on Brownian motion, an important class of first-passage processes is based on jump processes with scale-free, power-law distributed jump lengths. Thus, Lévy flights

* Corresponding author at: School of Mathematics and Statistics, Northwestern Polytechnical University, Xi'an 710072, China.
E-mail address: hsux3@nwpu.edu.cn (Y. Xu).

https://doi.org/10.1016/j.jcp.2021.110264
0021-9991/

and Lévy walks [22–24] have been promoted as efficient search mechanisms due to their interplay of local and non-local search patterns [25]. This efficiency is engrained in the so-called Lévy foraging hypothesis [26]. Lévy search patterns have, inter alia, been observed in the motion patterns of individual albatross birds [27] or marine predators [28]. They have been proposed for the optimal search by robots [29] and observed in human motion patterns [30]. Recently, Lévy spreading patterns have been revealed in the COVID-19 pandemic [31]. Theoretically, Lévy motion patterns may emerge due to dimensional reduction [32,33] or emerge from deterministic nonlinear systems near a critical point [34]. The efficiency of Lévy search-like patterns was studied in detail in, e.g., [33,35–38] for symmetric processes and in the presence of an external drift, e.g., wind or an underwater water stream [39,40]. The Lévy flight foraging hypothesis is a driving force for much research on ongoing Lévy flight search. In recent years, Reynolds explored the mechanisms behind the Lévy movement by analyzing movement patterns of marine predators, bacteria, honeybees, etc. [41]. Coherently Klages illustrated the need to go beyond the Lévy foraging hypothesis by elaborating on search for food of birds, fish and insects [42].

It has been realized that Lévy is not always optimal for all search situations. Simon and Julien indicated that a composite Brownian walks outperform a Lévy walk when the resources encountered are systematically detected [43]. Random search processes purely based on Lévy search mechanisms in some sense are hampered by the intrinsic property of leapover [44]: the searcher may overshoot the target point considerably. Consequently first-passage and first-arrival acquire significantly different behaviors for Lévy search processes [44–46]. The reduced arrival probability for Lévy searchers may be mitigated by adding a second motion mechanism, namely, continuous Brownian motion [47,48]. Such combined Lévy-Brown search in fact occurs naturally in physical scenarios of molecular-diffusive search in reduced-dimensional settings [32,33]. In models for gene regulation, for instance, long, Lévy-like jumps across chemically distant but physically close DNA-segments are followed by Brownian sliding motion along the DNA chain [33,47]. Combined Lévy and Brownian search was applied to food search by animals [49] and movement patterns of marine predators [28]. In such search processes, Lévy search patterns are efficient when the target is far from the starting point, while the Brownian search mechanism is advantageous for close-by targets. Combined dynamics of Gaussian and Lévy noises is also found in models for climate systems [50,51], in which the climate dynamics is affected by both atmospheric forcing and extreme climate. Atmospheric forcing, for instance, by wind stress, heating, and freshwater transport, is modeled as Gaussian noise, but extreme climate changes are modeled in terms of Lévy white noise. For the study of all these systems, the first-passage dynamics is of great interest: when does molecule bind to its specific spot on the DNA to start follow up reactions, or how long does it take until an animal located a food source or reach unoccupied territory? How long does it take for the population in a given geographical region to be infected by a virus? Or when would we expect a given climate parameter to reach above-critical values?

Here we study in detail the first-passage behavior of stochastic processes driven by combined Lévy-Gaussian white noise. We quantify the dynamics in terms of the first-passage probability, the first-passage time probability density function (PDF), and the mean first-passage time. In addition to these quantities, we will also study the reliability function to be defined below which is complementary to the first passage probability. The reliability function essentially represents the probability that no first-passage occurs within a given time interval and is thus directly related to what in physics literature is called the survival probability. The reliability function is the cumulative density function of the reliability density function (RDF), that represents the transient solution of the corresponding Fokker-Planck-Kolmogorov (FPK) equation with absorbing boundary conditions. The FPK equation is a deterministic method to study dynamics, similar to research on distributed space-fractional diffusion in anomalous kinetics, the Voigt function in spectroscopy, fractional advection diffusion in diffusion, etc. [52–57]. However, the analytical solution of the FPK equation only exists for a few special cases. For most cases, the FPK equation is solved numerically [58–60], for instance, by finite difference methods, finite element methods, the path integral (PI) method, etc. Among these, the PI method can obtain the transient solutions with high accuracy.

Once formulated for a specific system, the PI approach is very well suited for numerical evaluations of given stochastic differential equations (SDEs) or the corresponding FPK equations. It is important to emphasize that the PI solutions are highly accurate both in the transient and stationary cases. For SDEs solely driven by Gaussian, Poisson, or Lévy white noise, the PI method has been developed and investigated. Wehner and Wolfer solve the FPK equation corresponding to an SDE with Gaussian noise by the PI method firstly [61–63]. This method has been widely used to solve practical systems and improved by interpolation methods for higher accuracy [64–67]. Recently, the PI method has been extended to SDEs with non-Gaussian, Poisson or Lévy noise. The extension of the PI method for SDEs with Poisson white noise can be found in [68,69]. For the Lévy white noise case, the PI method was proved to be applicable to SDEs and the corresponding governing equations [70,71]. Moreover, the PI method has also been extended to solve SDEs with both Gaussian and Poisson noises [72]. Here we demonstrate how to extend the PI method to SDEs driven by both Gaussian and Lévy white noises.

In this paper, we study the first-passage dynamics of SDEs with both parametric Gaussian and additive Lévy white noises by extending the PI method to this case. The remainder of this paper is arranged as follows. Firstly, section 2 describes the model, which contains the SDEs and the corresponding FPK equations. Secondly, the extension of the PI method for the model is presented in section 3. Thirdly, in section 4 the performance indices of the first-passage problem are listed and the PI solutions are modified to allow the calculation of the performance indices. Then, in section 5, the PI solutions are calculated and are verified by extensive Monte Carlo simulations. Moreover, the first-passage problem for a range of different parameters is studied. Finally, section 6 concludes the paper. Details of the extension of the PI method to SDEs with combined parametric Gaussian and parametric Lévy white noises are presented in the Appendix.

2. The model

This section depicts the SDEs and the corresponding fractional FPK equations. The SDEs with both parametric Gaussian and additive Lévy noises are described in detail in section 2.1. In section 2.2, we derive the corresponding fractional FPK equations, which govern the PDFs of the solutions of the SDEs. The SDEs we used here is a stochastic differential equation in the Itô sense. For SDEs in the Stratonovich sense, we can transform the SDEs to Itô sense by use of the Wong-Zakai correction term. For more details, see [73] and the discussion with references in [74].

2.1. Stochastic differential equation

The scalar Itô SDE with Gaussian parametric noise and Lévy external noise reads

$$\begin{cases} \dot{X}(t) = f(X) + g(X)\xi(t) + \xi_\alpha(t), \\ X(0) = X_0, \end{cases} \tag{1}$$

where $\xi(t)$ and $\xi_\alpha(t)$ are Gaussian and α-stable Lévy white noises, respectively, and both noise sources are considered to be independent from another. Moreover, $f(X)$ and $g(X)$ are functions of X, and X_0 is the initial value of $X(t)$ at time $t = t_0$, which can be a deterministic or random variable with a given PDF. The "noise strength" $g(X)$ for non-constant $g(\cdot)$ is considered as multiplicative noise. Finally, the function $f(X)$ can be interpreted as a physical force, for instance, due to a finite territory of the searching animal.

The characteristic function of the α-stable Lévy white noise $\xi_\alpha(t)$ is $Z(k) = \exp(-D_L t|k|^\alpha)$, here and below, x is the variable in real space and k is the variable in the corresponding Fourier space. Here D_L and α are the noise intensity and stability index of the α-stable Lévy white noise, respectively. $\xi_\alpha(t)$ is the formal time derivative of a symmetric Lévy stable processes $L_\alpha(t)$. In Eq. (1), $\xi(t)$ is a Gaussian white noise with zero mean and the autocorrelation $\langle \xi(t)\xi(s)\rangle = 2D_G\delta(t-s)$, where D_G is the intensity of the Gaussian white noise and $\delta(\cdot)$ is the Dirac delta function. We note that $\xi(t)$ is the formal time derivative of Brownian motion $B(t)$. Next, we introduce the increment of the solution $X(t)$ in a sufficiently small time increment δt as $\delta X(\delta t)$. Namely, $\delta X(\delta t) = X(t+\delta t) - X(t)$. We will introduce the corresponding cumulant generating function $\delta K_X(k, \delta t|x, t)$ of the increment $\delta X(\delta t)$, which is needed for the derivation of the corresponding FPK equations.

For the increment $\delta X(\delta t)$ the corresponding characteristic function $\delta Z_X(k, \delta t|x, t)$ and the cumulant generating function $\delta K_X(k, \delta t|x, t)$ can be expressed as [75]

$$\begin{aligned} \delta Z_X(k, \delta t\,|y, t) &= \exp\left[\delta K_X(k, \delta t\,|y, t)\right] = \mathbb{E}\left\{\exp\left[ik\left(X(t+\delta t) - X(t)\right)\right]|X(t) = y\right\} \\ &= \mathbb{E}\left\{\exp\left[ikf(y)\delta t + ik\delta L + ikg(y)\delta B\right]|X(t) = y\right\} \\ &= \exp\left[ikf(y)\delta t\right]\mathbb{E}\left[\exp\left(ikg(y)\delta B\right)\right]\mathbb{E}\left[\exp\left(ik\delta L\right)\right]. \end{aligned} \tag{2}$$

In the above equation, k is the conjugate variable of $x - y$. Moreover, the δB and δL are increments of Brownian motion and the Lévy stable process, respectively.

For the Lévy stable process $L_\alpha(t)$, the increment δL and the corresponding characteristic function $\delta Z_L(k, \delta t)$ and cumulant generating function $\delta K_L(k, \delta t)$ satisfy

$$\delta Z_L(k, \delta t) = \exp\left[\delta K_L(k, \delta t)\right] = \mathbb{E}\left[\exp\left(ik\delta L\right)\right] = \exp\left[-\delta t D_L|k|^\alpha\right]. \tag{3}$$

For the Brownian motion $B(t)$, a similar relation among increment δB, characteristic function δZ_B and cumulant generating function δK_B reads

$$\delta Z_B(k, \delta t) = \exp\left[\delta K_B(k, \delta t)\right] = \mathbb{E}\left[\exp\left(ik\delta B\right)\right] = \exp\left[-\delta t D_G k^2\right]. \tag{4}$$

Using Eqs. (3) and (4), expression (2) is recast into

$$\delta Z_X(k, \delta t\,|y, t) = \exp\left[ikf(y)\delta t\right]\exp\left[-\delta t D_G k^2 g(y)^2\right]\exp\left[-\delta t D_L|k|^\alpha\right]. \tag{5}$$

Thus, the cumulant generating function $\delta K_X(k, \delta t|x, t)$ can be obtained as

$$\delta K_X(k, \delta t\,|y, t) = ikf(y)\delta t - \delta t D_G k^2 g(y)^2 - \delta t D_L|k|^\alpha. \tag{6}$$

2.2. Corresponding Fokker-Planck-Kolmogorov equation

In this subsection, the fractional FPK equations corresponding to the SDEs (1) are derived starting from the Chapman-Kolmogorov-Smoluchowski (CKS) equation and using the characteristic function. From Eq. (1) it follows immediately that the process $X(t)$ is Markovian (due to both Lévy process and Brownian motion with independent increments), thus the CKS equation holds. Namely, for $\forall \delta t > 0$ we have

$$p\left(x,t+\delta t\,|x_0,t_0\right)=\int_{-\infty}^{+\infty}p\left(x,t+\delta t\,|y,t\right)p\left(y,t\,|x_0,t_0\right)dy. \tag{7}$$

In the above equation, $p(x,t+\delta t|x_0,t_0)$ and $p(y,t|x_0,t_0)$ are the PDFs at times $t+\delta t$ and t with $x(t_0)=x_0$ as the initial value. Moreover, $p(x,t+\delta t|y,t)$ is the transition PDF from time t to $t+\delta t$ and from location y to x. By inverse Fourier transform $\mathscr{F}^{-1}$, the transition PDF $p(x,t+\delta t|y,t)$ in Eq. (7) can be expressed as

$$\begin{aligned}p(x,t+\delta t|y,t)&=\mathscr{F}^{-1}[\delta Z_X(k,\delta t|y,t)]=\mathscr{F}^{-1}[\exp(\delta K_X(k,\delta t|y,t))]\\&=\frac{1}{2\pi}\int_{-\infty}^{+\infty}\exp\left[-ik\left(x-y\right)\right]\exp\left[\delta K_X\left(k,\delta t\,|y,t\right)\right]dk.\end{aligned} \tag{8}$$

Inserting Eq. (8) into Eq. (7), we get

$$p\left(x,t+\delta t\,|x_0,t_0\right)=\frac{1}{2\pi}\int_{-\infty}^{+\infty}\int_{-\infty}^{+\infty}\exp\left[-ik\left(x-y\right)+\delta K_X\left(k,\delta t\,|y,t\right)\right]p\left(y,t\,|x_0,t_0\right)dkdy. \tag{9}$$

Letting $\delta t=0$, Eq. (9) reduces to

$$p\left(x,t\,|x_0,t_0\right)=\frac{1}{2\pi}\int_{-\infty}^{+\infty}\int_{-\infty}^{+\infty}\exp\left[-ik\left(x-y\right)\right]p\left(y,t\,|x_0,t_0\right)dkdy. \tag{10}$$

Subtracting Eq. (10) from expression (9) we have

$$\begin{aligned}&p\left(x,t+\delta t\,|x_0,t_0\right)-p\left(x,t\,|x_0,t_0\right)\\&=\frac{1}{2\pi}\int_{-\infty}^{+\infty}\int_{-\infty}^{+\infty}\left\{\exp\left[-ik\left(x-y\right)\right]\left[\exp\left(\delta K_X\left(k,\delta t\,|y,t\right)\right)-1\right]\right\}p\left(y,t\,|x_0,t_0\right)dkdy\\&=\frac{1}{2\pi}\int_{-\infty}^{+\infty}\int_{-\infty}^{+\infty}\left\{\exp\left[-ik\left(x-y\right)\right]\left[\delta K_X\left(k,\delta t\,|y,t\right)+\mathrm{O}\left(\delta t^2\right)\right]\right\}p\left(y,t\,|x_0,t_0\right)dkdy\\&=\int_{-\infty}^{+\infty}\mathscr{F}^{-1}\left[\delta K_X\left(k,\delta t\,|y,t\right)\right]p\left(y,t\,|x_0,t_0\right)dy+\mathrm{O}\left(\delta t^2\right).\end{aligned} \tag{11}$$

Here $\mathscr{F}^{-1}[\delta K_X(k,\delta t|y,t)]$ can be calculated through Eq. (6) as

$$\mathscr{F}^{-1}[\delta K_X(k,\delta t|y,t)]=f\left(y\right)\delta t\left(-1\right)\delta'\left(x-y\right)-\delta tD_Gg(y)^2\left(-\Delta\right)\delta\left(x-y\right)-\delta tD_L(-\Delta)^{\alpha/2}\delta\left(x-y\right). \tag{12}$$

Next, substituting Eq. (12) into relation (11), we get

$$\begin{aligned}&p\left(x,t+\delta t\,|x_0,t_0\right)-p\left(x,t\,|x_0,t_0\right)\\&=-\delta t\frac{\partial}{\partial x}\left(f\left(x\right)p\left(x,t\,|x_0,t_0\right)\right)+\delta tD_G\left(\Delta g(x)^2p\left(x,t\,|x_0,t_0\right)\right)-\delta tD_L\left((-\Delta)^{\alpha/2}p\left(x,t\,|x_0,t_0\right)\right)+O\left(\delta t^2\right).\end{aligned} \tag{13}$$

Thus, we get the corresponding governing equation

$$\begin{aligned}\frac{\partial}{\partial t}p\left(x,t\,|x_0,t_0\right)&=\lim_{\delta t\to0}\frac{p\left(x,t+\delta t\,|x_0,t_0\right)-p\left(x,t\,|x_0,t_0\right)}{\delta t}\\&=-\frac{\partial}{\partial x}\left[f\left(x\right)p\left(x,t\,|x_0,t_0\right)\right]+D_G\left[\Delta g(x)^2p\left(x,t\,|x_0,t_0\right)\right]-D_L\left[(-\Delta)^{\alpha/2}p\left(x,t\,|x_0,t_0\right)\right]\\&=-\frac{\partial}{\partial x}\left[f\left(x\right)p\left(x,t\,|x_0,t_0\right)\right]+D_G\frac{\partial^2}{\partial x^2}\left[g(x)^2p\left(x,t\,|x_0,t_0\right)\right]+D_L\frac{\partial^\alpha}{\partial|x|^\alpha}p\left(x,t\,|x_0,t_0\right).\end{aligned} \tag{14}$$

Equivalently, the PDF $p\left(x,t\right)$ of the solution of Eq. (1) satisfies

$$\frac{\partial}{\partial t}p\left(x,t\right)=-\frac{\partial}{\partial x}\left[f\left(x\right)p\left(x,t\right)\right]+D_G\frac{\partial^2}{\partial x^2}\left[g(x)^2p\left(x,t\right)\right]+D_L\frac{\partial^\alpha}{\partial|x|^\alpha}p\left(x,t\right), \tag{15}$$

with the initial condition $p(x,t_0)=\delta(x-x_0)$ or an assigned PDF. In addition, the fractional FPK equation (15) can be directly inferred from the continuous time random walk theory under combined Gaussian and Lévy walk [47,48,76]. In Eq. (15) the fractional operator $\partial^\alpha/\partial|x|^\alpha\cdot$ is understood in terms of its Fourier transform $-|k|^\alpha\cdot$ [76]. Eq. (15) can be viewed as a generalized case, as:

(i) For $D_L=0$ Eq. (15) becomes

$$\frac{\partial}{\partial t}p\left(x,t\right)=-\frac{\partial}{\partial x}\left[f\left(x\right)p\left(x,t\right)\right]+D_G\frac{\partial^2}{\partial x^2}\left[g(x)^2p\left(x,t\right)\right], \tag{16}$$

which is the governing equation of the SDE with parametric Gaussian noise.

(ii) For $D_G=0$ Eq. (15) reduces to

$$\frac{\partial}{\partial t}p\left(x,t\right)=-\frac{\partial}{\partial x}\left[f\left(x\right)p\left(x,t\right)\right]+D_L\frac{\partial^\alpha}{\partial|x|^\alpha}p\left(x,t\right). \tag{17}$$

This is just the fractional FPK equation corresponding to SDE with α-stable Lévy white noise [76–78].

3. Path integral solution

This section is about the extension of the PI method to the SDEs (1) as well as the corresponding fractional FPK equations (15). Specifically, the short-time transition PDF is derived in detail. The PI solution obtained through this short-time transition PDF then is shown to satisfy the fractional FPK equation (15), which corroborates the correctness of the short-time transition PDF.

The PI method is an effective method to calculate the evolution of the resulting processes in terms of the short-time transition PDF in a step-by-step fashion. The PDF $p(x,t)$ of $X(t)$ can be obtained through

$$p\left(x,t\right)=\int_R p\left(x,t\,|x_0,t_0\right)p\left(x_0,t_0\right)dx_0, \tag{18}$$

where $p(x_0,t_0)$ is the initial PDF of $X(t)$ at $t=t_0$. Dividing the time interval $[t_0,t]$ into N sub-intervals, we have

$$p\left(x,t\right)=\int_R p\left(x,t\,|x_{N-1},t_{N-1}\right)\int_R p\left(x_{N-1},t_{N-1}\,|x_{N-2},t_{N-2}\right)\cdots\int_R p\left(x_1,t_1\,|x_0,t_0\right)p\left(x_0,t_0\right)dx_0\cdots dx_{N-2}dx_{N-1}, \tag{19}$$

where $t_0<t_1<t_2<\ldots<t_N=t$. This expression indicates that the long-term evolution is composed of a series of short-term evolutions. This means that the transient PDFs can be obtained starting from a given initial condition (deterministic or stochastic) once the short-time transition PDF is obtained.

3.1. Short-time transition PDF

Although the solution of the fractional FPK equations (15) is just the short-time transition PDFs (for sufficiently small $t-t_0$), it is quite difficult to solve this kind of fractional FPK equations analytically. To overcome this difficulty, we derive the short-time transition PDFs through the SDEs (1) directly using the ideas developed in [68–70,72], which are depicted in Fig. 1.

In Fig. 1, the trajectories $\bar{X}(\rho)$, starting from the deterministic point $\bar{x}$, are trajectories from the whole set of trajectories of the processes $X(t)$ in the short-time interval $[t,t+\delta t]$. These trajectories still satisfy the SDE (1) and can be depicted as

$$\begin{cases}\dot{\bar{X}}\left(\rho\right)=f\left(\bar{X}\right)+g\left(\bar{X}\right)\xi\left(t+\rho\right)+\xi_\alpha\left(t+\rho\right),\\ \bar{X}\left(0\right)=\bar{x}.\end{cases}\qquad(0<\rho\le\delta t) \tag{20}$$

Therefore, the short-time transition PDF $p(x,t+\delta t|\bar{x},t)$ of the process $X(t)$ in Eq. (1) coincides with the unconditional PDF $p_{\bar{X}}(x,\delta t)$ of the process $\bar{X}(\rho)$, namely, $p(x,t+\delta t|\bar{x},t)=p_{\bar{X}}(x,\delta t)$.

Despite the fact that the conditional PDFs can be derived through the unconditional PDFs, the derivation is still not easy. The transition PDFs for the combined Gaussian and Poisson white noises can be derived due to a particularity of Poisson white noise [72]. Different from Poisson white noise, Lévy white noise is defined through its characteristic function, such that we do not have similar access to a corresponding short-time transition PDFs for combined Gaussian and Lévy white noises. Moreover, it is apparent that the characteristic function of combined Gaussian and Lévy white noises cannot be expressed by a new α-stable distribution due to the different stability parameters. As stated by Nadarajah that the sum of random variables is a stable random variable only when the two random variable components have the same stability parameter α [79]. Thus, we cannot directly find the short-time transition PDFs through the characteristic function of α-stable Lévy noises. In order to obtain these, the characteristic functions and their properties for Gaussian and Lévy white noises are used. The derivation goes as follows.

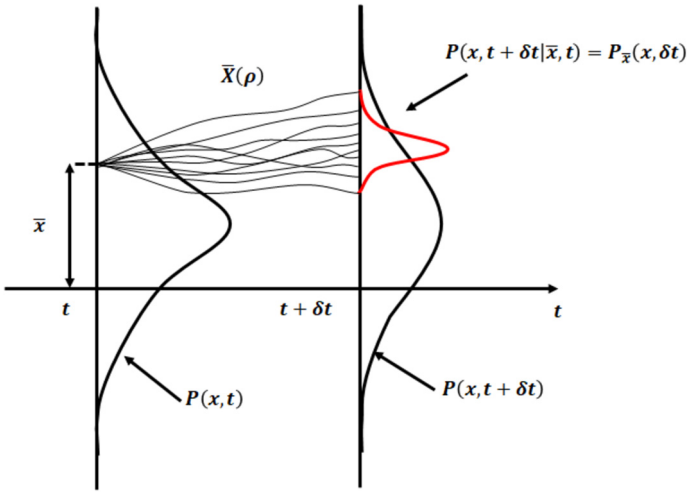

Fig. 1. Sample functions of $\bar{X}(\rho)$ and conditional PDF.

From the perspective of the whole trajectory $X(t)$, the trajectory $\bar{X}(\rho)$ is approximately linear due to the small value of δt. In this small interval, the increment $dB(t)$ of Brownian motion is a random variable that satisfies a Gaussian distribution with intensity $2D_G$. Moreover the increment $dL_\alpha(t)$ of Lévy process is random variable with intensity D_L and stability parameter α. Then, $\bar{X}(\delta t)$ can be approximated as

$$\bar{X}(\delta t)=\bar{x}+f(\bar{x})\,\delta t+g(\bar{x})\,dB(t)+dL_\alpha(t). \tag{21}$$

According to the characteristic function of $dL_\alpha(t)$ and $dB(t)$ in Eqs. (3) and (4), as well as the properties of the characteristic function, we can get the characteristic function of $\bar{X}(\delta t)$ in the form

$$Z_{\bar{X}}(k,\delta t)=\exp\left(ik\bar{x}+ikf(\bar{x})\,\delta t-D_G\delta tk^2g(\bar{x})^2-D_L\delta t|k|^\alpha\right), \tag{22}$$

which is the Fourier transform of the unconditional PDF $p_{\bar{X}}(x,\delta t)$.

Then, we get the conditional PDF as follows

$$\begin{aligned}p(x,t+\delta t|\bar{x},t)&=p_{\bar{X}}(x,\delta t)=\mathscr{F}^{-1}\left(Z_{\bar{X}}(k,\delta t)\right)=\frac{1}{2\pi}\int_{-\infty}^{+\infty}\exp(-ikx)Z_{\bar{X}}(k,\delta t)\,dk\\&=\frac{1}{2\pi}\int_{-\infty}^{+\infty}\exp(-ikx)\exp\left(ik\bar{x}+ikf(\bar{x})\,\delta t-D_G\delta tk^2g(\bar{x})^2-D_L\delta t|k|^\alpha\right)dk.\end{aligned} \tag{23}$$

This short-time solution can be regarded as a general case of the following two particular cases:

(i) In the Gaussian noise case ($D_L=0$)

$$\begin{aligned}p(x,t+\delta t|\bar{x},t)&=\frac{1}{2\pi}\int_{-\infty}^{+\infty}\exp(-ikx)\exp\left(ik\bar{x}+ikf(\bar{x})\,\delta t-D_G\delta tk^2g(\bar{x})^2\right)dk\\&=\frac{1}{2\pi\sqrt{D_Gg(\bar{x})^2\delta t}}\exp\left[-\frac{(-x+\bar{x}+f(\bar{x})\,\delta t)^2}{4D_Gg(\bar{x})^2\delta t}\right],\end{aligned} \tag{24}$$

this is just the short-time solution of the SDE with Gaussian white noise [1,80].

(ii) In the Lévy noise case ($D_G=0$)

$$p(x,t+\delta t|\bar{x},t)=\frac{1}{2\pi}\int_{-\infty}^{+\infty}\exp(-ikx)\exp\left(ik\bar{x}+ikf(\bar{x})\,\delta t-D_L\delta t|k|^\alpha\right)dk, \tag{25}$$

this is the short-time solution of the SDE solely driven by white Lévy noise [70,71].

3.2. Verification of the short-time transition PDF

In this section, the correctness of the short-time transition PDF is verified. Specifically, starting from the CKS equation where the short-time transition PDF (23) is used, we get the fractional FPK equation (15).

According to the CKS equation, the PDF $p(x,t+\delta t)$ can be expressed by the conditional PDF $p(x,t+\delta t|\bar{x},t)$ and its previous moment's PDF $p(\bar{x},t)$ as

$$p\left(x,t+\delta t\right)=\int_{-\infty}^{+\infty}p\left(x,t+\delta t|\,\bar{x},t\right)p\left(\bar{x},t\right)d\bar{x}=\int_{-\infty}^{+\infty}\mathscr{F}^{-1}\left(Z_{\bar{X}}\left(k,\delta t\right)\right)p\left(\bar{x},t\right)d\bar{x}. \tag{26}$$

Its Fourier transform can be obtained as

$$\begin{aligned}Z_X\left(k,t+\delta t\right)&=\mathscr{F}\left[p\left(x,t+\delta t\right)\right]=\int_{-\infty}^{+\infty}Z_{\bar{X}}\left(k,\delta t\right)p\left(\bar{x},t\right)d\bar{x}\\&=\exp\left(-D_L\delta t|k|^{\alpha}\right)\int_{-\infty}^{+\infty}\exp\left(-D_G\delta tk^2g(\bar{x})^2+ik\bar{x}+ikf\left(\bar{x}\right)\delta t\right)p\left(\bar{x},t\right)d\bar{x}.\end{aligned} \tag{27}$$

For the integral we find

$$\begin{aligned}&\int_{-\infty}^{+\infty}\exp\left(-D_G\delta tk^2g(\bar{x})^2+ik\bar{x}+ikf\left(\bar{x}\right)\delta t\right)p\left(\bar{x},t\right)d\bar{x}\\&=\int_{-\infty}^{+\infty}\exp\left(ik\bar{x}\right)\exp\left[ikf\left(\bar{x}\right)\delta t-D_G\delta tk^2g(\bar{x})^2\right]p\left(\bar{x},t\right)d\bar{x}\\&=\int_{-\infty}^{+\infty}\exp\left(ik\bar{x}\right)\left[1+ikf\left(\bar{x}\right)\delta t-D_G\delta tk^2g(\bar{x})^2\right]p\left(\bar{x},t\right)d\bar{x}+O\left(\delta t^2\right)\\&=\int_{-\infty}^{+\infty}\exp\left(ik\bar{x}\right)p\left(\bar{x},t\right)d\bar{x}+\int_{-\infty}^{+\infty}\exp\left(ik\bar{x}\right)\left[ikf\left(\bar{x}\right)\delta t\right]p\left(\bar{x},t\right)d\bar{x}\\&\quad-\int_{-\infty}^{+\infty}\exp\left(ik\bar{x}\right)\left[D_Gk^2\delta tg(\bar{x})^2\right]p\left(\bar{x},t\right)d\bar{x}+O\left(\delta t^2\right)\\&=Z_X\left(k,t\right)+\mathbb{E}\left[\exp\left(ikx\right)ikf\left(x\right)\delta t\right]-\mathbb{E}\left[\exp\left(ikx\right)D_Gk^2g(x)^2\delta t\right]+O\left(\delta t^2\right).\end{aligned} \tag{28}$$

The Taylor series expansion of $\exp(-D_L\delta t|k|^{\alpha})$ about δt is $\exp(-D_L\delta t|k|^{\alpha})=1-D_L\delta t|k|^{\alpha}+O(\delta t^2)$. Thus, Eq. (27) can be rewritten as

$$\begin{aligned}&Z_X\left(k,t+\delta t\right)\\&=\left[1-D_L\delta t|k|^{\alpha}+O\left(\delta t^2\right)\right]\left\{Z_X\left(k,t\right)+\mathbb{E}\left[\exp\left(ikx\right)ikf\left(x\right)\delta t\right]-\mathbb{E}\left[\exp\left(ikx\right)D_Gk^2\delta tg(x)^2\right]+O\left(\delta t^2\right)\right\}\\&=Z_X\left(k,t\right)+ik\delta t\mathbb{E}\left[\exp\left(ikx\right)f\left(x\right)\right]-D_Gk^2\delta t\mathbb{E}\left[\exp\left(ikx\right)g(x)^2\right]-D_L|k|^{\alpha}\delta tZ_X\left(k,t\right)+O\left(\delta t^2\right).\end{aligned} \tag{29}$$

Rewriting Eq. (29) and taking the limit $\delta t\to 0$, we get

$$\begin{aligned}\frac{\partial Z_X\left(k,t\right)}{\partial t}&=\lim_{\delta t\to 0}\frac{Z_X\left(k,t+\delta t\right)-Z_X\left(k,t\right)}{\delta t}\\&=\left(-D_L|k|^{\alpha}\right)Z_X\left(k,t\right)+ik\mathbb{E}\left[\exp\left(ikx\right)f\left(x\right)\right]-D_Gk^2\mathbb{E}\left[\exp\left(ikx\right)g(x)^2\right].\end{aligned} \tag{30}$$

After inverse Fourier transform, Eq. (30) becomes

$$\frac{\partial p\left(x,t\right)}{\partial t}=-\frac{\partial}{\partial x}\left[f\left(x\right)p\left(x,t\right)\right]+D_G\frac{\partial^2}{\partial x^2}\left[g(x)^2p\left(x,t\right)\right]+D_L\frac{\partial^{\alpha}}{\partial|x|^{\alpha}}p\left(x,t\right), \tag{31}$$

which is same as the fractional FPK equation (15). Thus, the correctness of the short-time transition PDF is verified.

4. First-passage time statistics from path integral solutions

In this section, we modify the PI solutions to characterize the first-passage problem. The key to analyzing the first-passage problem by PI solutions consists in defining the so-called reliability density function (RDF). The RDF is the PDF that the trajectories remain away from the absorbing boundary condition until the observation time [70,72]. In physical terms the cumulative reliability is called the survival probability.

Specifically, let $[\eta, \zeta]$ denote the threshold barriers. The barriers are absorbing boundary conditions, at which the trajectories need to be eliminated once they cross these barriers. This indicates that the RDF outside the "safe domain" must be zero. Considering that the initial condition in Eq. (1) can be a deterministic value or a random variable, the RDF $q_{\eta\zeta}(x, 0)$ at the initial time step can be calculated through the PDF $p(x, 0)$ by neglecting the part outside the safe area. This property can be expressed as

$$q_{\eta\zeta}(x, 0) = U(x - \eta)\, U(\zeta - x)\, p(x, 0), \tag{32}$$

where $U(\cdot)$ denotes the Heaviside function. Moreover, the RDF in a generic time instant $t + \delta t$ is given as

$$q_{\eta\zeta}(x, t + \delta t) = U(x - \eta)\, U(\zeta - x) \int_{\eta}^{\zeta} p(x, t + \delta t \,|\bar{x}, t)\, q_{\eta\zeta}(\bar{x}, t)\, d\bar{x}, \tag{33}$$

where the RDF $q_{\eta\zeta}(\bar{x}, t)$ at a former time instant t is used to avoid that trajectories return to the safe domain after having left before. The Heaviside function $U(\cdot)$ is used again to neglect the trajectories, which first cross the safe domain during time interval $[t, t + \delta t]$. This definition states that the RDF $q_{\eta\zeta}(x, t)$ is an monotonically non-increasing function of time t. Eqs. (32) and (33) can be viewed as modification of the PI solutions. The RDF can be derived through the modified formulas directly. Moreover, through the RDF, we can derive other first-passage performance indices, such as the reliability function $R(T)$ at time T, the first-passage time PDF $p_f(T)$ and the mean first-passage time.

The reliability function $R(T)$ is the probability that the process stays inside the interval $[\eta, \zeta]$ over the time interval $[0, T]$. We can get the reliability function by integrating the RDF as follows,

$$R(T) = \int_{\eta}^{\zeta} q_{\eta\zeta}(x, T)\, dx. \tag{34}$$

Obviously, the complement of the reliability function is the first-passage probability $P_F(T)$, which is the probability that the process crosses the barriers over the time interval $[0, T]$. Then, the PDF of the first-passage time $p_f(T)$ can be obtained as

$$p_f(T) = \frac{dP_F(T)}{dT} = -\frac{dR(T)}{dT}. \tag{35}$$

The first-passage time is a random variable and its first order moment is often used to define the degree of reliability. It is called the mean first-passage time (MFPT) and is defined as

$$\mathrm{MFPT} = \mathbb{E}[T] = \int_{0}^{\infty} T\, p_f(T)\, dT. \tag{36}$$

In our approach, the RDF is calculated by discretizing the aforementioned formulas (32) and (33). The two formulas can be viewed as a modification of the PI solutions. Then, the other performance indices can be obtained via equations (34), (35), and (36).

5. Numerical results

In this section, simulation results are presented to show that the PI method is applicable to SDEs with both parametric Gaussian and additive Lévy white noises. Namely, the PI method can get the PDFs of this kind of SDEs or solve the corresponding fractional FPK equations. Moreover, the influences of the system parameters on the first-passage problem are analyzed through PI solutions. In all figures, the results from direct Monte Carlo simulations of the original SDEs (1) are also given to verify the PI solutions. All Monte Carlo results in this paper are calculated with time step $dt = 0.0001$, space resolution $dx = 0.01$, and 8×10^6 sample paths for deterministic initial condition while 32×10^6 sample paths for Gaussian-distributed initial condition. Specifically, a single sample path is obtained by the forward Euler formula as

$$x(t + dt) = x(t) + f(x)\, dt + g(x)\, \xi(t) dt^{1/2} + \xi_{\alpha}(t)\, dt^{1/\alpha}, \tag{37}$$

where $\xi(t)$ is a white Gaussian random variable with zero mean and variance $2D_G$, and $\xi_{\alpha}(t)$ is a white stable random variable with stability parameter α and intensity D_L. Given the time t, the PDF and RDF is derived by dividing the space interval with space increment $dx = 0.01$ and counting the sample points on each space cell.

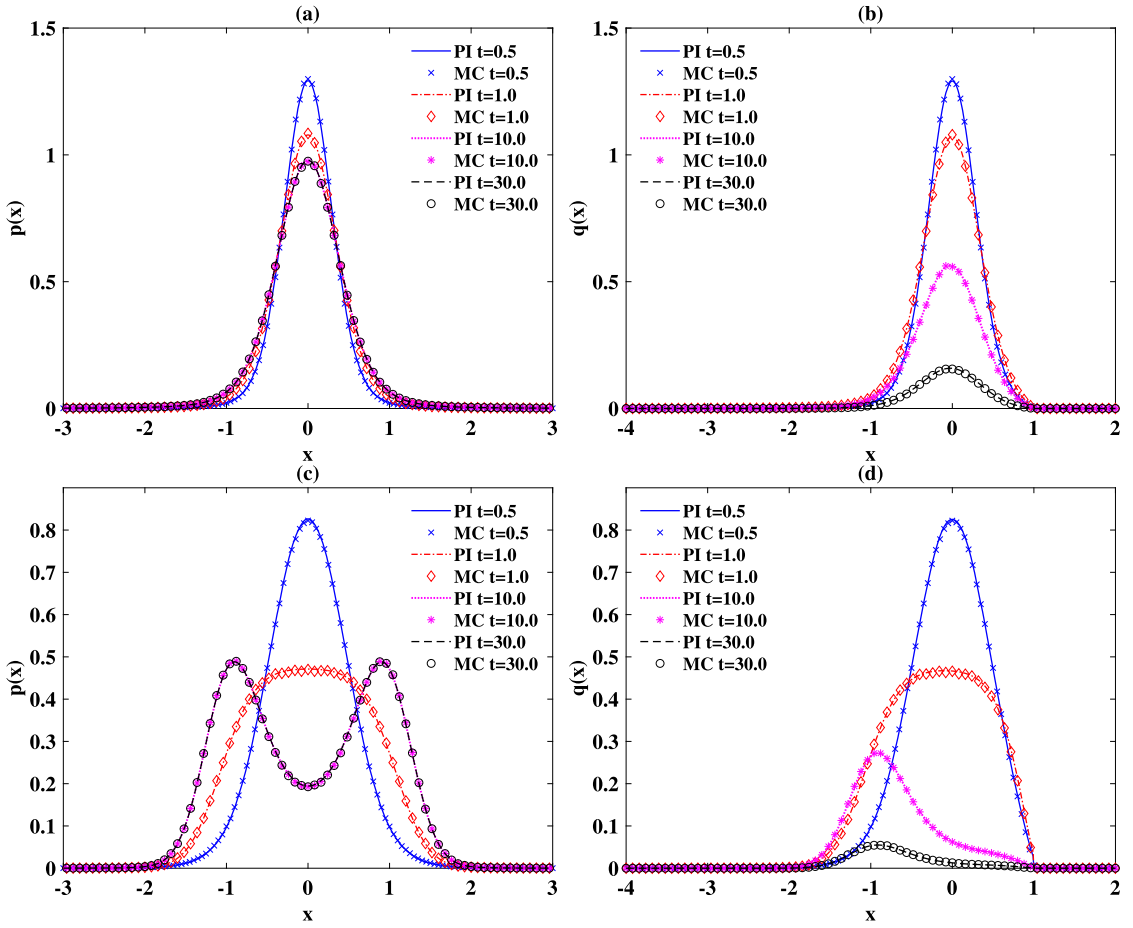

Fig. 2. PDFs and RDFs for deterministic initial condition. (a, b) are for $a = 1.0$, $b = 0.0$, $c = 0.5$, $\alpha = 1.5$, and $D_L = D_G = 0.1$. (c, d) are for $a = -1.0$, $b = c = 1.0$, $\alpha = 1.5$, and $D_L = D_G = 0.1$. The left panels show the PDFs and the right panels the RDFs. For the RDFs in (b, d) the absorbing barriers are selected as $\eta = -4$ and $\zeta = 1$ (PI: path integral solution, MC: Monte Carlo solution). (For interpretation of the colors in the figures, the reader is referred to the web version of this article.)

5.1. Validity of the path integral method

In this part, the validity of the PI method for solving the fractional FPK equations (15) (or obtaining the PDFs from the SDEs (1)) is presented for the concrete case $f(x) = -ax - bx^3$ and $g(x) = \sqrt{1 + cx^2}$. Our model here is derived from a climate system [50,51], in which the climate information can be characterized by the calcium (Ca) signal in ice cores. Specifically, we will get the PDFs of the process $X(t)$ for the following SDEs (Itô sense)

$$\begin{cases} \dot{X}(t) = -aX - bX^3 + \sqrt{1 + cX^2}\xi(t) + \xi_\alpha(t) \\ X(0) = X_0 \end{cases} \tag{38}$$

where the initial value X_0 can be deterministic or a random variable with assigned PDF. In other words, we will get the solutions of the corresponding fractional FPK equations

$$\frac{\partial p(x,t)}{\partial t} = \frac{\partial}{\partial x}\left[\left(ax + bx^3\right)p(x,t)\right] + D_G\frac{\partial^2}{\partial x^2}\left[\left(1 + cx^2\right)p(x,t)\right] + D_L\frac{\partial^\alpha}{\partial |x|^\alpha}p(x,t), \tag{39}$$

with the initial condition $p(x, t_0) = \delta(x - x_0)$ or other assigned forms. Next, our simulation results for two different initial conditions are presented. The two initial conditions are deterministic and Gaussian-distributed, respectively.

5.1.1. Example 1: Deterministic initial condition

The deterministic initial condition $X(0) = X_0$, or equivalently $p(x, t_0) = \delta(x - x_0)$ is selected. The PDF and the RDF are calculated through the PI iteration (7) and its modification (33), respectively. The results are presented in Fig. 2 and the excellent agreement between the PI solutions and Monte Carlo solutions supports the validity of the PI method.

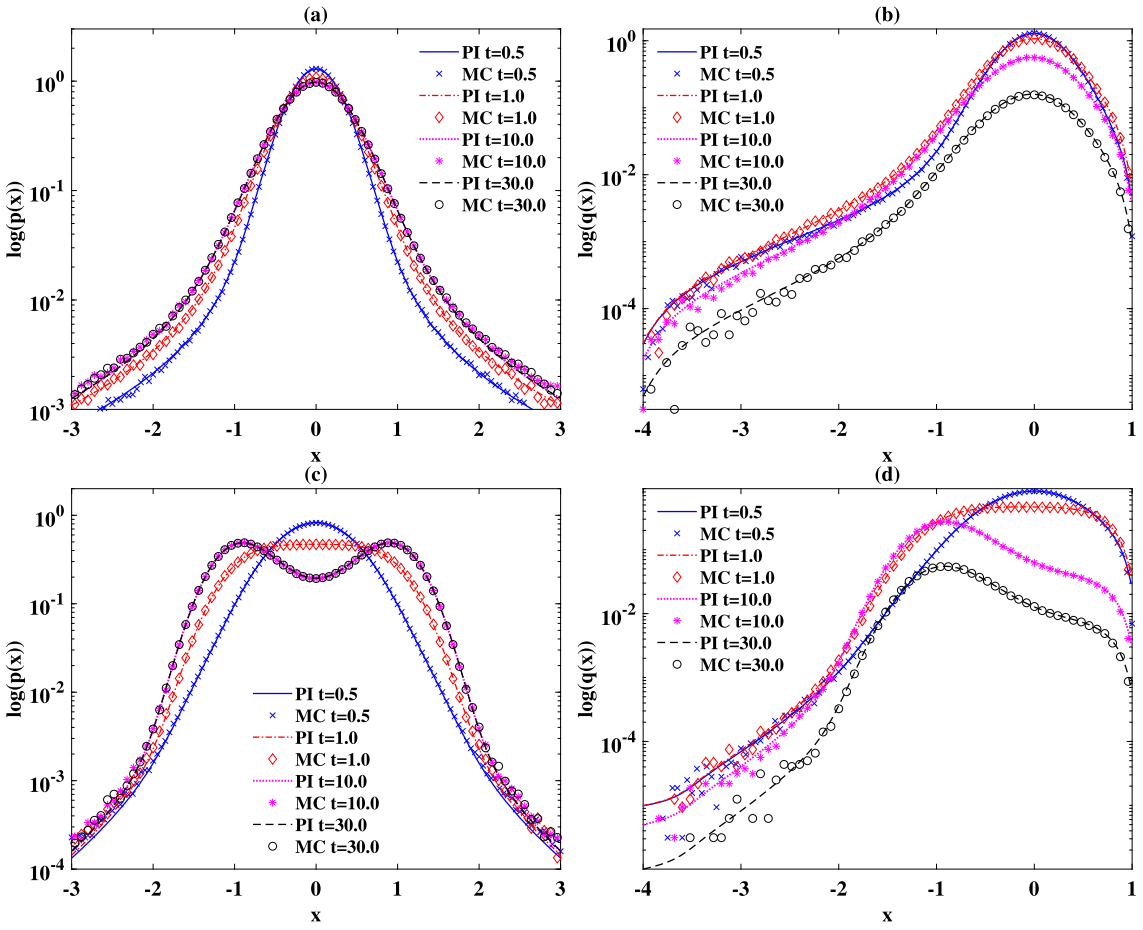

Fig. 3. Log-linear plots of the PDFs and RDFs for deterministic initial condition corresponding to Fig. 2. (a, b) are for $a = 1.0$, $b = 0.0$, $c = 0.5$, $\alpha = 1.5$, and $D_L = D_G = 0.1$. (c, d) are for $a = -1.0$, $b = c = 1.0$, $\alpha = 1.5$, and $D_L = D_G = 0.1$. The left panels show the PDFs and the right panels the RDFs. (PI: path integral solution, MC: Monte Carlo solution).

We choose two different sets of parameters. Fig. 2 (a, b) are for one parameter set, and Fig. 2 (c, d) are for the other. Different parameter sets lead to different solutions: the stationary solution in Fig. 2 (a) is unimodal while that in Fig. 2 (c) is bimodal. For each parameter set, the PDFs on the left reach a stationary state at $t = 30$, but the RDFs on the right keep changing with time due to the absorbing barrier. Note that in order to better display the zero value of the RDFs outside the reliability domain $[\eta, \zeta] = [-4, 1]$, we show the RDFs for the interval $[-4, 2]$. In our calculations, considering the independence of different sample paths, we divide the 8×10^6 sample paths into 100 copies, each copy with 8×10^4 sample paths. Finally a set of calculation results is obtained through 1.16273×10^4 s (about 3.22 h) for parameters $a = 1.0, b = 0.0, c = 0.5$ and 1.07881×10^4 s (about 2.99 h) for another set of parameters. Similarly, different points are independent of each other in the path integral transition probability density function, we run 500 points in parallel at a time and it takes 2.57626×10^3 s (about 0.77 h) to get the result for parameters $a = 1.0, b = 0.0, c = 0.5$ and 2.59285×10^3 s (about 0.72 h) for another set. In Fig. 3, the PDFs and RDFs are also presented on a log-linear scale. These semi-logarithmic plots make it easy to see details for small values of PDFs and RDFs. It can be observed that the PDFs and RDFs fit well at a very low magnitude (about 10^{-6} to 10^{-4}). To further quantify the accuracy of the PI solution, by taking the Monte Carlo solution as the standard solution, we define the L_2 error norm as

$$L_2 = \frac{\{\sum_{i,j}[P_{PI}(x_i, t_j) - P_{MC}(x_i, t_j)]^2\}^{1/2}}{\{\sum_{i,j}[P_{MC}(x_i, t_j)]^2\}^{1/2}}, \tag{40}$$

where P_{PI} is the numerical PI solution and P_{MC} is Monte Carlo solution. For the two cases $a = 1.0, b = 0.0, c = 0.5$ and $a = -1.0, b = c = 1.0$ used in Fig. 2, their L_2 error norm are 0.003981 and 0.006888, respectively. A smaller value of L_2 indicates a better accuracy of the PI solution.

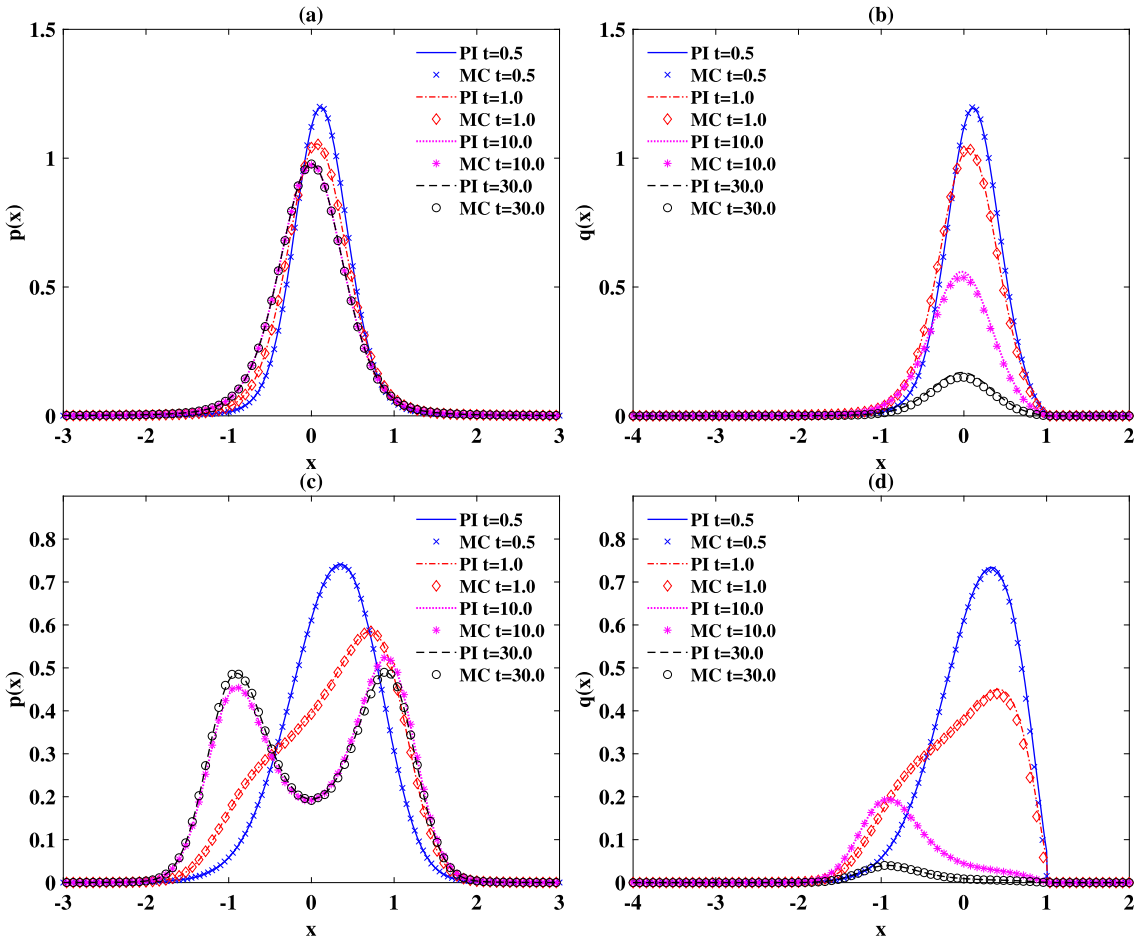

Fig. 4. PDFs and RDFs for Gaussian initial condition. (a, b) are for $a = 1.0$, $b = 0.0$, $c = 0.5$, $\alpha = 1.5$, and $D_L = D_G = 0.1$. (c, d) are for $a = -1.0$, $b = c = 1.0$, $\alpha = 1.5$, and $D_L = D_G = 0.1$. The left panels show the PDFs and the right panels the RDFs. For the RDF in (b, d) the absorbing barriers are chosen as $\eta = -4$ and $\zeta = 1$ (PI: path integral solution; MC: Monte Carlo solution).

5.1.2. Example 2: Gaussian initial condition

Now, we assume that the initial condition x_0 is a random variable chosen from the Gaussian distribution

$$p\,(x_0, 0) = \frac{1}{\sqrt{2\pi}\sigma} \exp\left[-\frac{(x_0 - \mu)^2}{2\sigma^2}\right], \tag{41}$$

with $\mu = 0.2$ and $\sigma = 0.2$. Then, we calculate the PDFs and RDFs by the PI method, starting from this Gaussian initial condition and using the same two sets of parameters as in Example 1. In addition, the Monte Carlo solutions of the original SDEs are also calculated for comparison. In our calculation, the computational cost for the Monte Carlo solutions is necessarily high to ensure the same smoothness as in the deterministic initial condition.

Fig. 4 presents the PDFs and RDFs for Gaussian initial conditions for two different sets of parameters. The good agreement between the PI solutions and Monte Carlo results in each plot indicates that the PI method works very well. Fig. 4 (a, b) are for one set of parameters and Fig. 4 (c, d) for the other parameter set. Analogously to the deterministic initial condition, the PDFs approach a stationary state, while the RDFs keep changing with time for each parameter set. Again we show the RDFs in the domain $[-4, 2]$ to better display the zero value of the RDFs outside the reliability domain $[\eta, \zeta] = [-4, 1]$. In addition, comparing the PDFs in Example 1 and Example 2, we find that the initial conditions have no significant effect on the stationary solutions due to the uniqueness of the solution for the stationary FPK equation, as it should be. In our calculations, 32×10^6 sample paths are divided into 400 copies, and each copy with 8×10^4 sample paths, the calculation time for $a = 1.0, b = 0.0, c = 0.5$ and $a = -1.0, b = c = 1.0$ are 1.25206×10^4 s (about 3.4 h) and 1.26368×10^4 s (about 3.5 h), respectively. Similarly, we run 500 points in parallel at a time to get the PI solution, and it takes 2.59224×10^3 s (about 0.72 h) and 2.49794×10^3 s (about 0.69 h) for parameters $a = 1.0, b = 0.0, c = 0.5$ and the other set. Again, the log-linear plots of the PDFs and RDFs are presented in Fig. 5 to show that PI is accurate at very low magnitudes. Moreover,

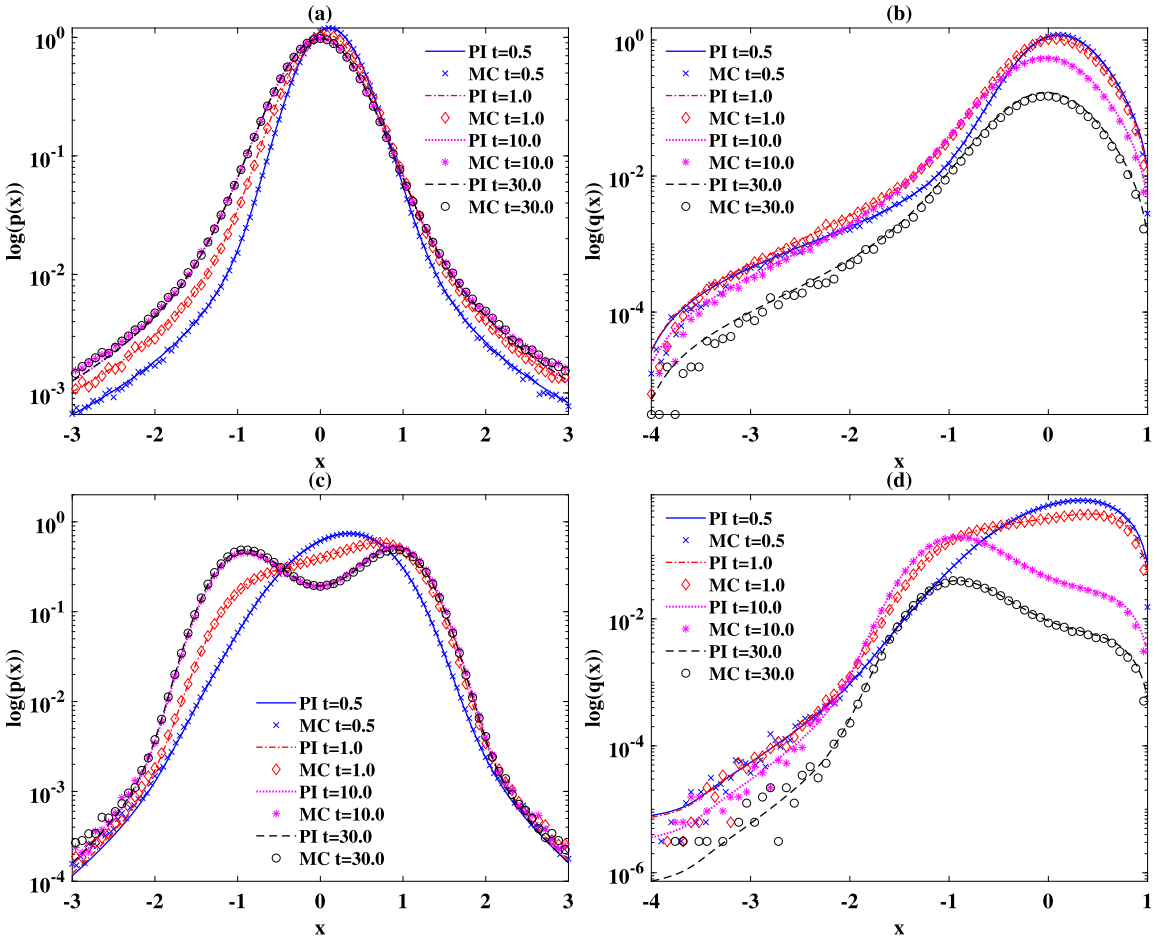

Fig. 5. Log-linear plots of PDFs and RDFs for Gaussian initial condition, corresponding to Fig. 4. (a, b) are for $a = 1.0$, $b = 0.0$, $c = 0.5$, $\alpha = 1.5$, and $D_L = D_G = 0.1$. (c, d) are for $a = -1.0$, $b = c = 1.0$, $\alpha = 1.5$, and $D_L = D_G = 0.1$. The left panels show the PDFs and the right panels the RDFs. (PI: path integral solution; MC: Monte Carlo solution).

the L_2 error norm are 0.004208 and 0.007774 for the cases $a = 1.0, b = 0.0, c = 0.5$ and $a = -1.0, b = c = 1.0$, respectively. The smaller L_2 error norm is consistent with the good fitting results.

5.2. First-passage statistics

After verifying the validity of the PI method, the influence of the system parameters on the first-passage statistics is analyzed based on the modified PI formula (33) in this section. The modified PI solutions under different noise intensities, barriers, and stability parameters are calculated and presented. The pertinent Monte Carlo solutions of the original SDEs (38) are also contained for comparison. For simplicity, only the most commonly used deterministic initial condition is considered.

5.2.1. Case 1: dependence on noise intensities

Fig. 6 presents the reliability functions and first-passage time PDFs for different noise intensities. Fig. 6 (a, b) are for different Gaussian noise intensities D_G and Fig. 6 (c, d) are for different noise intensities D_L. For each noise intensity, the reliability functions indicate that the initial condition $x(0)$ is completely within the reliability interval with the reliability function $R(t) = 1.0$. As time increases, $R(t)$ decreases nonlinearly to zero, where the process $x(t)$ is completely gone from the reliability interval. Since $R(t)$ depends nonlinearly on t, there is a time when the decay of the reliability function occurs most rapidly. This time is just the point where the first-passage time PDF $P_f(t)$ assumes its maximum. The solid points in the first-passage PDF curve reveal the time that the process is most likely outside the reliability interval. For different noise intensities, Fig. 6 shows that both D_L and D_G have a strong influence on the reliability function and the first-passage time PDF, respectively. Fig. 6 (a) and (c) indicate that the reliability is higher for smaller noise intensities. The most likely first-passage time decreases as the noise intensity increases, as expected, see Fig. 6 (b) and (d).

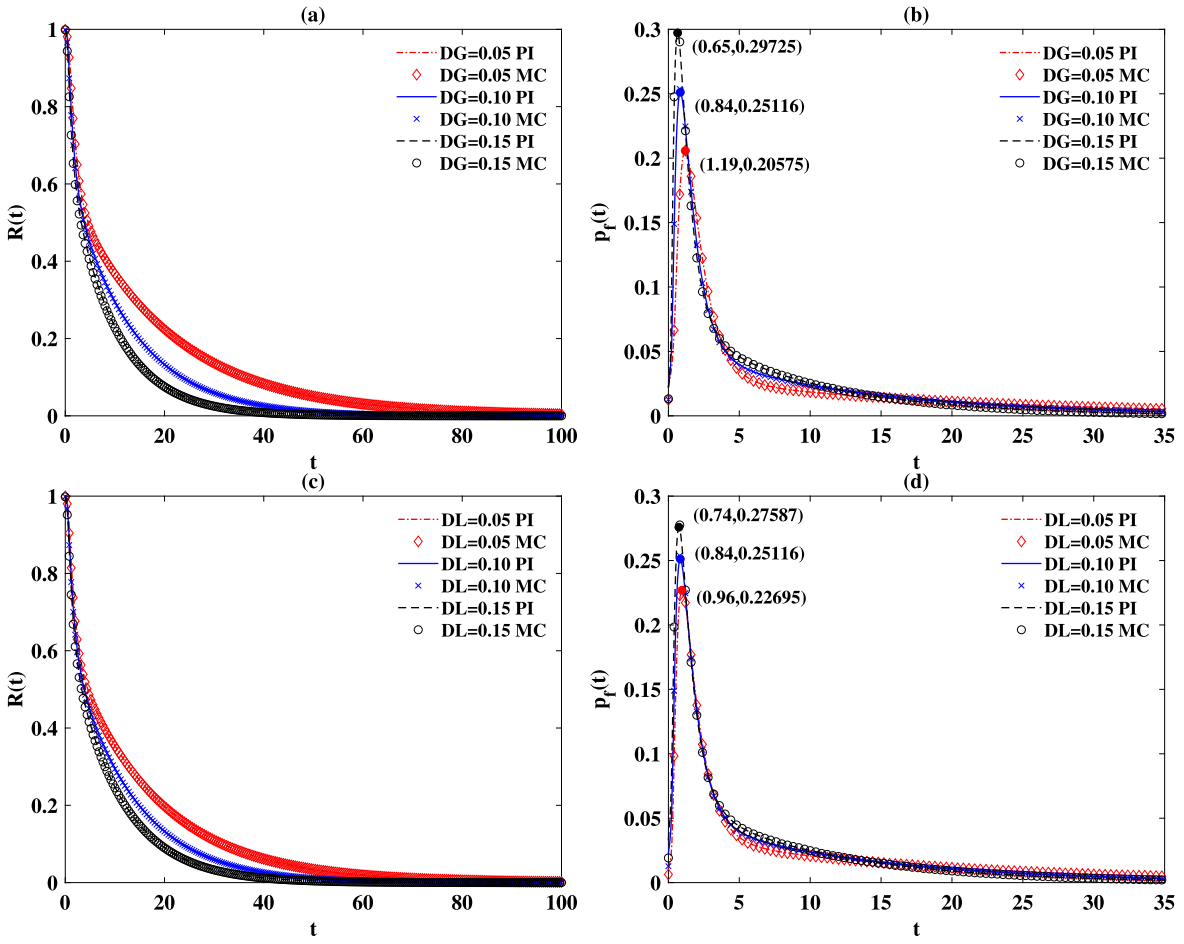

Fig. 6. Reliability functions and first-passage time PDFs for different noise intensities, for parameters $a = -1.0$, $b = c = 1.0$, $\alpha = 1.5$, $\eta = -4$, and $\zeta = 1$. (a, b) are for different D_G with $D_L = 0.1$; (c, d) are for different D_L with $D_G = 0.1$ (PI: path integral solution; MC: Monte Carlo solution).

Additionally, the results of Fig. 6 are presented on log-linear scale in Fig. 7. Analogously, Fig. 7 (a, b) are for different Gaussian noise intensities D_G and Fig. 7 (c, d) are for different noise intensities D_L. In each plot, the Monte Carlo solution and PI solution agree well with each other, supporting the correctness of the results. Indeed, the PI solution is accurate to order less than 10^{-6} at the tails. To obtain the same accuracy more sample paths are needed for the Monte Carlo method. Importantly, the plots indicate that the logarithm of the reliability function, $\log(R(t))$, and the logarithm of the first-passage time PDFs, $\log(P_f(t))$, are inversely related to time t. This means that the reliability functions $R(t)$ and the first-passage time PDF $P_f(t)$ decrease exponentially with time, as expected for a Markovian process in a finite domain. The value $p_f(0)$ is the PDF that $x(t)$ jumps out of the reliability domain $[\eta = -4, \zeta = 1]$ with the first jump staring from the initial point. As can be seen, the value is non-zero, a characteristic of the non-local jumps made possible by the Lévy noise, see the related results for the first-passage time PDF of pure Lévy flights and walks in Ref. [46]. We also find that different noise intensities D_L or D_G lead to different decays of the reliability functions $R(t)$ and the first-passage time PDF $P_f(t)$: faster decay goes along with larger noise intensities.

In addition, the degree to which different noise intensities impact the results for the MFPT is shown in Fig. 8. The MFPT is obtained by the PI and Monte Carlo methods, and they agree well with each other. Fixing one of the noise intensities D_G or D_L, the increase of the another noise intensity causes a decrease of the MFPT. Namely, the MFPT is a decreasing function of the noise intensities, as expected. Moreover, the MFPT is more sensitive to changes of the noise intensity when D_L is fixed.

5.2.2. Case 2: dependence on barriers

Figs. 9 and 11 reveal the impact of the barrier positions on the first-passage problem. Fig. 9 presents the reliability functions and first-passage time PDFs with different barriers. Fig. 9 (a, b) are for several different left boundaries η with fixed right boundary $\zeta = 1$. Fig. 9 (a) shows that the closer the boundary η to the initial zero, the smaller the reliability function at the same time instant. Namely, the process needs less time to reach the boundary. Fig. 9 (c, d) presents a similar

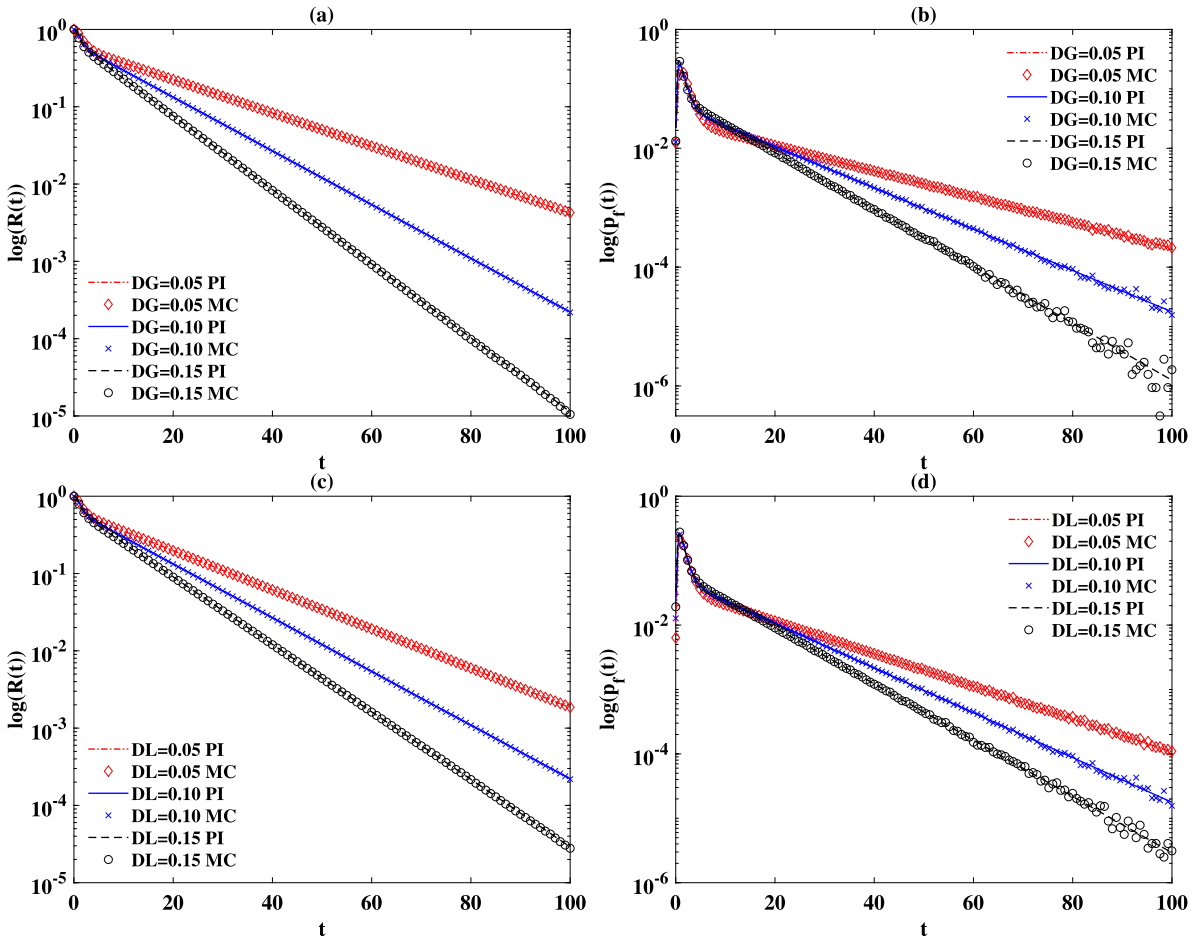

Fig. 7. Log-linear plots for the reliability functions and first-passage time PDFs for different noise intensities for parameters $a = -1.0$, $b = c = 1.0$, $\alpha = 1.5$, $\eta = -4$, and $\zeta = 1$. (a, b) are for different D_G with $D_L = 0.1$; (c, d) are for different D_L with $D_G = 0.1$ (PI: path integral solution; MC: Monte Carlo solution).

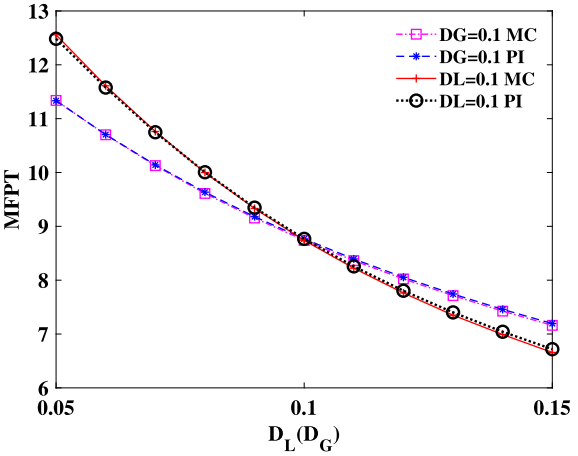

Fig. 8. MFPTs for different noise intensities for parameters $a = -1.0$, $b = c = 1.0$, $\alpha = 1.5$, $\eta = -4$, and $\zeta = 1$ (PI: path integral solution; MC: Monte Carlo solution).

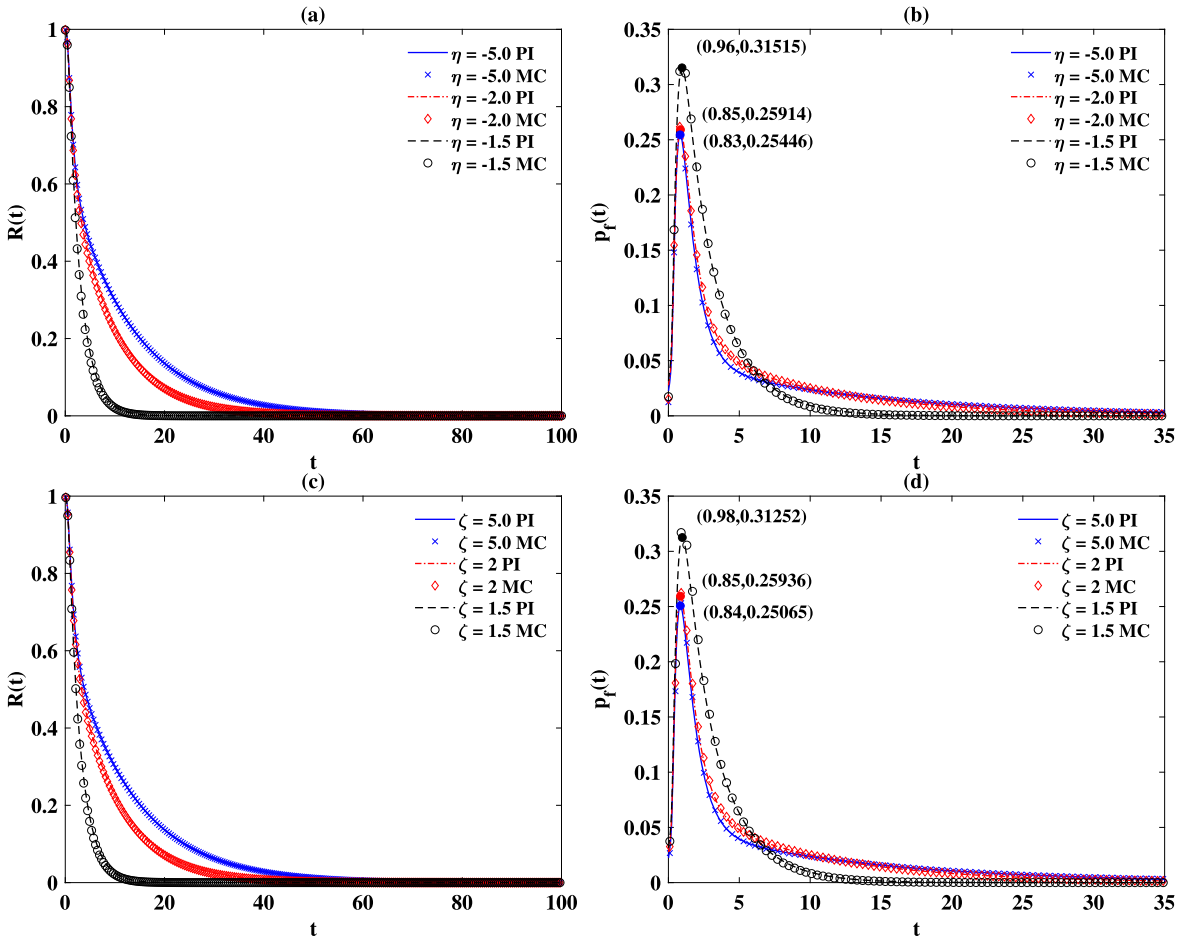

Fig. 9. Reliability functions and first-passage time PDFs for different barrier positions with parameters $a = -1.0$, $b = c = 1.0$, $\alpha = 1.5$, $D_L = D_G = 0.1$. (a, b) are for fixed right barrier $\zeta = 1$; (c, d) are for fixed left barrier $\eta = -1$ (PI: path integral solution; MC: Monte Carlo solution).

result for different right barrier positions ζ with a fixed left barrier $\eta = -1$. Moreover, the MFPT for different barriers are presented in Fig. 11. For fixed right barrier $\zeta = 1$, Fig. 11 (a) shows that closer barrier position η leads to smaller MFPT, as expected. For fixed left barrier $\eta = -1$, Fig. 11 (b) shows the analogous result for the right barrier.

Corresponding to Fig. 9 we present the results on log-linear scale in Fig. 10. Fig. 10 (a, b) are for several different left boundaries η with fixed right boundary $\zeta = 1$. Fig. 10 (c, d) present similar results for different right barriers ζ with a fixed left barrier $\eta = -1$. These plots indicate that the logarithm of the reliability functions $\log(R(t))$ and the logarithm of the first-passage time PDFs $\log(P_f(t))$ are inversely related to time t, i.e., the reliability functions $R(t)$ and the first-passage time PDF $P_f(t)$ decrease exponentially with time. Concurrently, a shorter safety interval length leads to faster decay. For the fastest cases ($\eta = -1.5$, $\zeta = 1$ or $\eta = -1.0$, $\zeta = 1.5$), the MC and PI results do not fit well when time t is too large. This is due to the fact that the Monte Carlo method is statistical in nature, and it is difficult to obtain an accurate estimate of small probability events.

5.2.3. *Case 3: dependence on stability parameter α*

In Fig. 12, the first-passage behavior is obtained from the PI method for different stability parameters α. Fig. 12 (a) shows the reliability functions and Fig. 12 (b) the PDFs of the first-passage time. Fig. 12 (a) shows that smaller stability indices lead to lower reliability function values at the same time. Indeed, one can see a crossover from higher first-passage probabilities at short times to the inverse behavior closer to the most likely time. A similar behavior was observed in [81,82]. Fig. 12 (b) presents the most probable time that the process crosses the barriers. Smaller α leads to longer most probable times. On the log-linear scale of Fig. 12, Fig. 13 shows a zoom into the plot for long times t and reveals the relationship. Good agreement of the MC results and the PI results is observed for all cases. Again, we see that the logarithm of the reliability functions $\log(R(t))$ and the logarithm of the first-passage time PDFs $\log(P_f(t))$ are inversely related to time t, i.e., the reliability functions $R(t)$ and the first-passage time PDF $P_f(t)$ decrease exponentially with time. The numerical results indicate that smaller α speeds up the decay. This is intuitive due to the fact that the jumps are longer for smaller α.

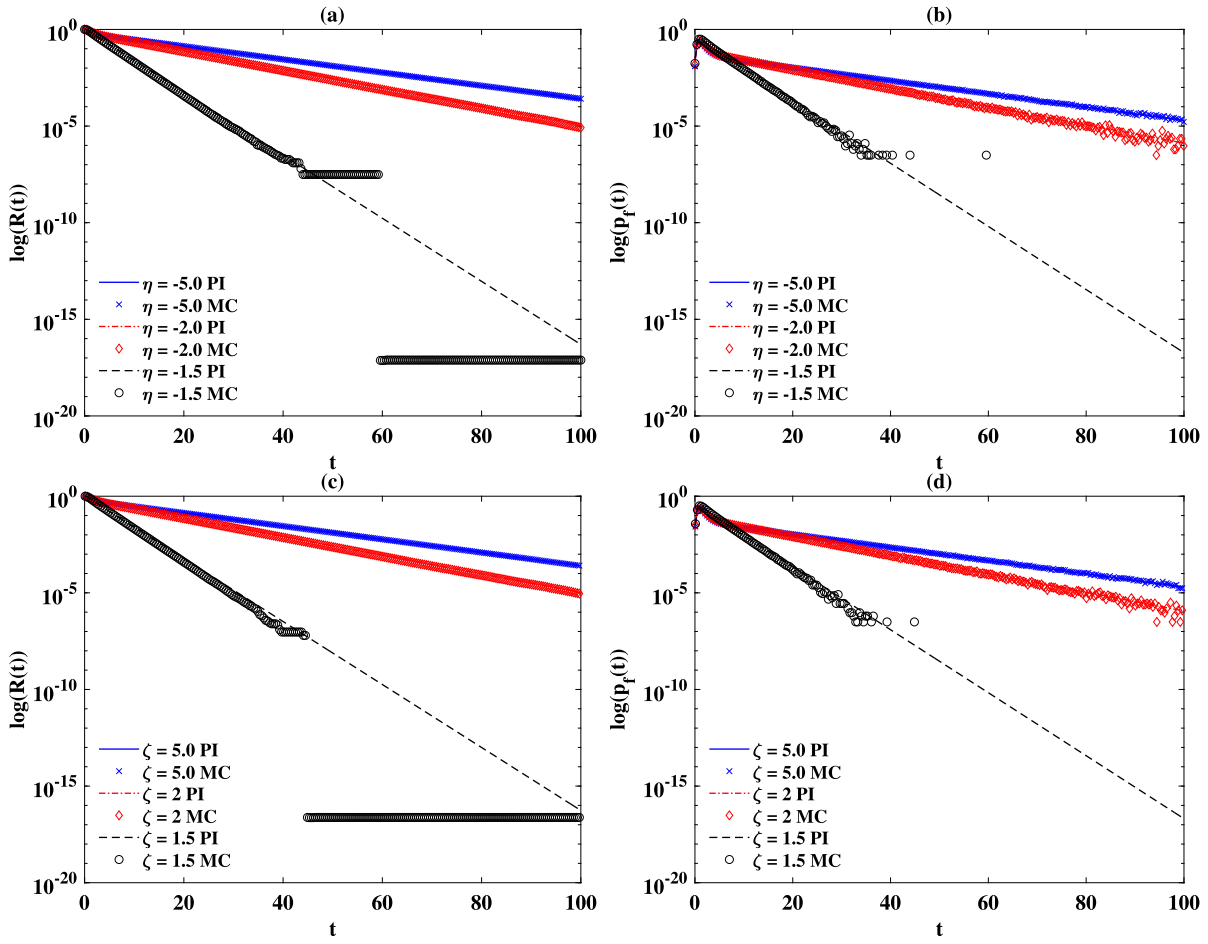

Fig. 10. Log-linear plots for reliability functions and first-passage time PDFs for different barrier values with parameters $a = -1.0$, $b = c = 1.0$, $\alpha = 1.5$, and $D_L = D_G = 0.1$. (a, b) are for fixed right barrier $\zeta = 1$; (c, d) are for fixed left barrier $\eta = -1$ (PI: path integral solution; MC: Monte Carlo solution).

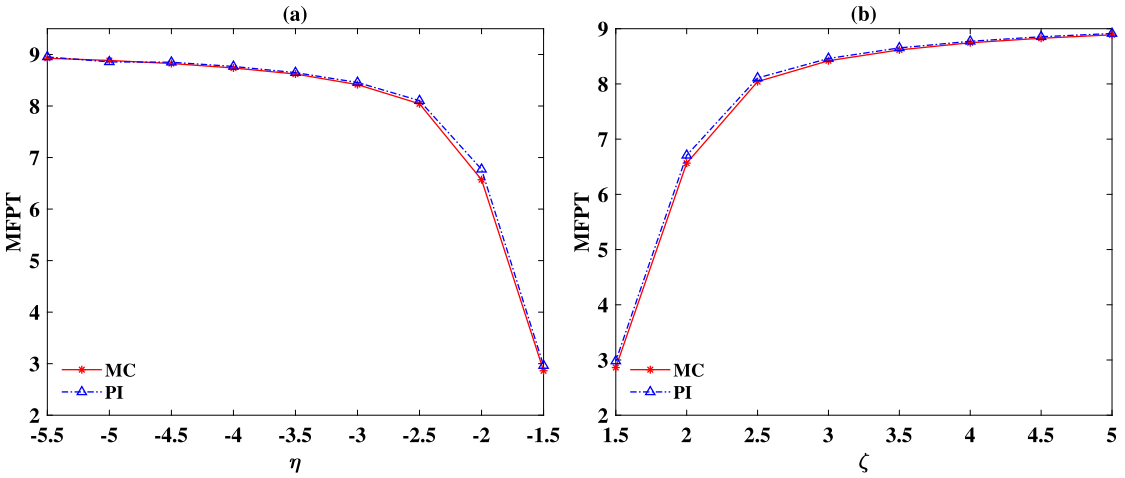

Fig. 11. MFPT for different barrier value for parameters $a = -1.0$, $b = c = 1.0$, $\alpha = 1.5$, and $D_L = D_G = 0.1$. (a) for fixed right barrier $\zeta = 1$; (b) for fixed left barrier $\eta = -1$ (PI: path integral solution; MC: Monte Carlo solution).

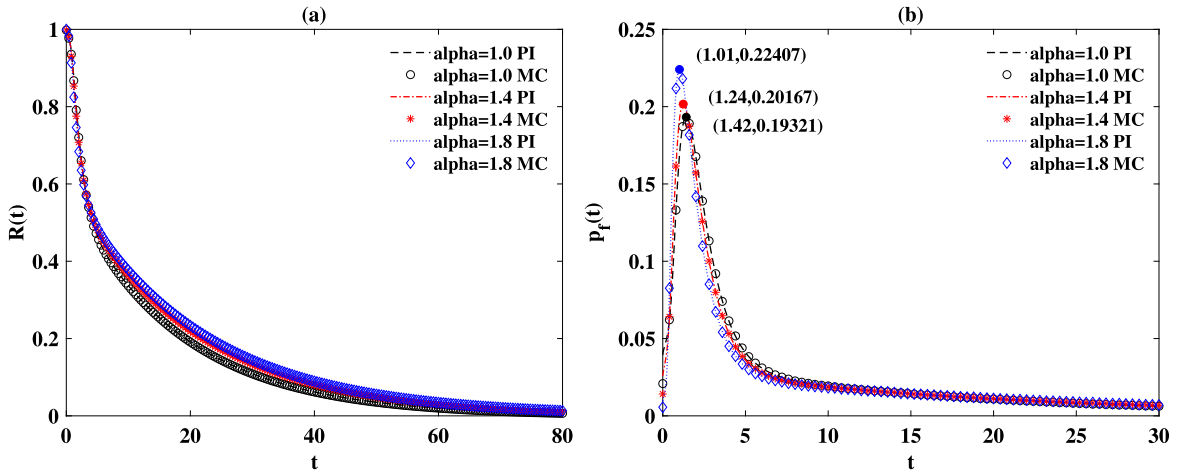

Fig. 12. Reliability functions and first-passage time PDFs for different stability parameters α with $a = -1.0$, $b = c = 1.0$, $D_L = 0.1$, $D_G = 0.05$, $\eta = -4$, and $\zeta = 1$ (PI: path integral solution; MC: Monte Carlo solution).

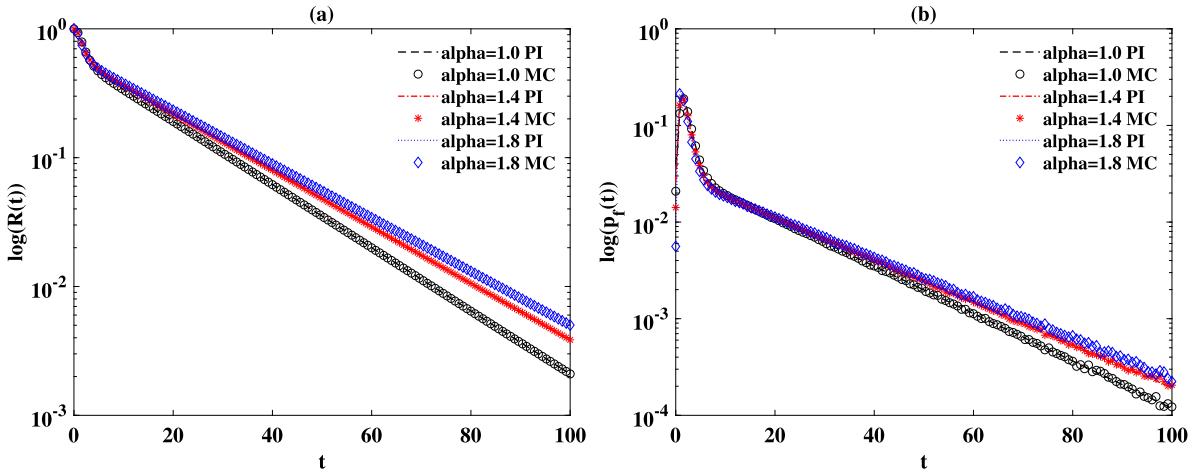

Fig. 13. Log-linear plots for the reliability functions and first-passage time PDFs for different stability parameters α with $a = -1.0$, $b = c = 1.0$, $D_L = 0.1$, $D_G = 0.05$, $\eta = -4$, and $\zeta = 1$ (PI: path integral solution; MC: Monte Carlo solution).

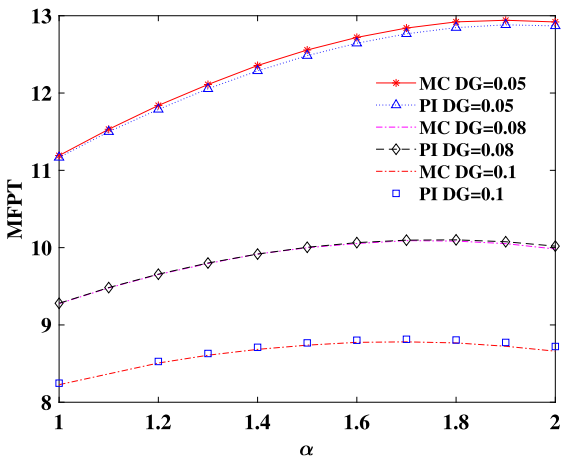

Fig. 14. MFPT for different stability parameters α and noise intensities D_G for parameters $a = -1.0$, $b = c = 1.0$, $D_L = 0.1$, $\eta = -4$, and $\zeta = 1$ (PI: path integral solution; MC: Monte Carlo solution).

Moreover, the MFPT for different stability parameters α is plotted in Fig. 14. We calculate three sets of different parameters (with different noise intensities D_G) to analyze the impact of the stability parameters on the MFPT. For any set of the parameters, the MFPT increases as the stability parameters α increase, which is more obvious to see for smaller D_G. Note that the MFPT does not increase monotonically when α increases. The study of the exact position of the apparent maxima of the MFPT for certain α is a topic of future work. In addition, for fixed α, the MFPT can be seen to be smaller when D_G is larger. This result is analogous to the result of Case 1.

6. Conclusions

In this paper we pursued two goals. In the first part we extend the PI method to SDEs with both parametric Gaussian and additive Lévy white noises and the corresponding fractional FPK equations. Specifically, short-time transition PDFs, which are used in the PI method, are derived from the SDEs. The fractional FPK equations corresponding to the SDEs are derived to verify the short-time transition PDFs. Based on different initial conditions and different system parameters, the PI solutions are implemented and agree well with Monte Carlo simulations. Thus, the PI method is applicable and indeed very efficient for this type of SDEs and the corresponding fractional FPK equations. The second part of this work concerns the modification of the PI solutions to analyze the first-passage problem. In section 5.2, we calculated the RDF, first-passage time PDF and the MFPT through the modified PI solutions, for different noise intensities, barriers and stability parameters. On average, the larger the noise intensity, the shorter the threshold barriers, and the smaller stability parameters will lead to a faster first-passage. Moreover, the comparison between the PI results and those from Monte Carlo simulations of the original SDEs indicates that the modification of the PI solutions yields highly accurate results.

We are confident that our conceptual results for the PI method and its application to first-passage problems will be useful in many applications. We finally note that while we analyzed a one-dimensional system here, generalization to higher dimensions is possible by combination of the component-wise PI solution.

CRediT authorship contribution statement

Wanrong Zan: Conceptualization, Funding acquisition, Methodology, Software, Writing – original draft, Writing – review & editing. **Yong Xu:** Conceptualization, Funding acquisition, Methodology, Project administration, Supervision, Writing – original draft, Writing – review & editing. **Ralf Metzler:** Conceptualization, Funding acquisition, Methodology, Writing – original draft, Writing – review & editing. **Jürgen Kurths:** Conceptualization, Funding acquisition, Methodology, Writing – original draft, Writing – review & editing.

Declaration of competing interest

The authors declare that they have no known competing financial interests or personal relationships that could have appeared to influence the work reported in this paper.

Acknowledgements

This paper was supported by the National Natural Science Foundation of China (No. 11772255, 12072264), the Fundamental Research Funds for the Central Universities, the Research Funds for Interdisciplinary Subject of Northwestern Polytechnical University, the Shaanxi Project for Distinguished Young Scholars, Shaanxi Provincial Key R&D Program (2020KW-013 and 2019TD-010) and National Key Research and Development Program of China (No. 2018AAA0102201). W.R. Zan was sponsored by Innovation Foundation for Doctor Dissertation of Northwestern Polytechnical University (No. CX202045). R. Metzler acknowledges funding from the German Research Foundation (DFG, Grant No. ME 1535/7-1) and the Foundation for Polish Science (Fundacja na rzecz Nauki Polskiej, FNP) within an Alexander von Humboldt Honorary Polish Research Scholarship. J. Kurths was supported by the project RF Government Grant 075-15-2019-1885.

Appendix. Extension of the PI method

We consider the extension of the PI method to SDEs with parametric Gaussian and Lévy white noise and its corresponding FPK equation,

$$\begin{cases} \dot{X}(t) = f(X) + g_1(X)\xi(t) + g_2(X)\xi_\alpha(t) \\ X(0) = X_0 \end{cases} \tag{42}$$

where $\xi(t)$ and $\xi_\alpha(t)$ are Gaussian and α-stable Lévy white noises respectively, and they are independent. Here, $f(X)$, $g_1(X)$ and $g_2(X)$ are functions of X, and X_0 is the initial value of $X(t)$ at time $t = t_0$, which can be deterministic or random variable with given PDF.

According to the derivation in section 2.2, we can get the fractional FPK equation corresponding to the SDE (42) as

$$\frac{\partial}{\partial t}p(x,t) = -\frac{\partial}{\partial x}\left[f(x)\,p(x,t)\right] + D_G\frac{\partial^2}{\partial x^2}\left[g_1(x)^2 p(x,t)\right] + D_L\frac{\partial^\alpha}{\partial|x|^\alpha}\left[|g_2(x)|^\alpha p(x,t)\right]. \tag{43}$$

Moreover, the short-time transition PDF for this case is obtained through the derivation presented in section 3.1 as

$$p_X(x, t+\delta t|\bar{x}, t) = \frac{1}{2\pi}\int_{-\infty}^{+\infty} \exp(-ikx)\exp\left(ik\bar{x} + ikf(\bar{x})\delta t - D_G\delta t k^2 g_1(\bar{x})^2 - D_L\delta t|k|^\alpha |g_2(\bar{x})|^\alpha\right) dk. \tag{44}$$

The short-time transition PDF is verified by a similar procedure in section 3.2. We can obtain the fractional FPK equation (43) starting from the CKS equation, where the short-time transition PDF is used. Finally, through the CKS equation, the PI solutions for the SDE with parametric Gaussian and Lévy noise (and corresponding FPK equation) can be written as

$$\begin{aligned} &p(x, t+\delta t) \\ &= \frac{1}{2\pi}\int_{-\infty}^{+\infty}\int_{-\infty}^{+\infty} \exp(-ikx)\exp\left(ik\bar{x} + ikf(\bar{x})\delta t - D_G\delta t k^2 g_1(\bar{x})^2 - D_L\delta t|k|^\alpha |g_2(\bar{x})|^\alpha\right) p(\bar{x}, t)\, dk d\bar{x}. \end{aligned} \tag{45}$$

Then, if a system can be modeled by an SDE with parametric Gaussian and Lévy noise, we can solve it through the extended PI method.

References

[1] J.Q. Sun, Stochastic Dynamics and Control, Elsevier, 2006.
[2] S. Redner, A Guide to First-Passage Processes, Cambridge University Press, 2001.
[3] N.G. Van Kampen, Stochastic Processes in Physics and Chemistry, Elsevier, 1992.
[4] Y.G. Li, Y. Xu, J. Kurths, J.Q. Duan, The influences of correlated spatially random perturbations on first passage time in a linear-cubic potential, Chaos, Interdiscip. J. Nonlinear Sci. 29 (2019) 101102.
[5] R. Metzler, G. Oshanin, S. Redner, First Passage Problems: Recent Advances, World Scientific, Singapore, 2014.
[6] H.C. Tuckwell, Stochastic Processes in the Neurosciences, SIAM, 1989.
[7] Z.C. Ren, W. Xu, D.L. Wang, Dynamic and first passage analysis of ship roll motion with inelastic impacts via path integration method, Nonlinear Dyn. 97 (2019) 391–402.
[8] S.T. Ariaratnam, W.C. Xie, Dynamic buckling of shallow curved structures under stochastic loads, Nonlinear Dyn. 8 (1995) 179–195.
[9] M. Potters, J.P. Bouchaud, Theory of Financial Risk and Derivative Pricing: From Statistical Physics to Risk Management, Cambridge University Press, 2003.
[10] M.V. Smoluchowski, Versuch einer mathematischen theorie der koagulationskinetik kolloider lösungen (Attempt on a mathematical theory of the kinetics of coagulation of colloidal solutions), Z. Phys. Chem. 92 (1917) 129–168.
[11] F.C. Collins, G.E. Kimball, Diffusion-controlled reaction rates, J. Colloid Sci. 4 (1949) 425–437.
[12] A.B. Kolomeisky, Physics of protein–DNA interactions: mechanisms of facilitated target search, Phys. Chem. Chem. Phys. 13 (2011) 2088–2095.
[13] O. Pulkkinen, R. Metzler, Distance matters: the impact of gene proximity in bacterial gene regulation, Phys. Rev. Lett. 110 (2013) 198101.
[14] O. Bénichou, C. Chevalier, J. Klafter, B. Meyer, R. Voituriez, Geometry-controlled kinetics, Nat. Chem. 2 (2010) 472.
[15] S. Condamin, O. Bénichou, V. Tejedor, R. Voituriez, J. Klafter, First-passage times in complex scale-invariant media, Nature 450 (2007) 77–80.
[16] C. Mejía-Monasterio, G. Oshanin, G. Schehr, First passages for a search by a swarm of independent random searchers, J. Stat. Mech. Theory Exp. 2011 (2011) P06022.
[17] T.G. Mattos, C. Mejía-Monasterio, R. Metzler, G. Oshanin, First passages in bounded domains: when is the mean first passage time meaningful?, Phys. Rev. E 86 (2012) 031143.
[18] A. Godec, R. Metzler, Universal proximity effect in target search kinetics in the few encounter limit, Phys. Rev. X 6 (2016) 041037.
[19] A. Godec, R. Metzler, First passage time statistics for two-channel diffusion, J. Phys. A, Math. Theor. 50 (2017) 084001.
[20] D.S. Grebenkov, R. Metzler, G. Oshanin, Strong defocusing of molecular reaction times results from an interplay of geometry and reaction control, Commun. Chem. 1 (2018) 1–12.
[21] D.S. Grebenkov, R. Metzler, G. Oshanin, Full distribution of first exit times in the narrow escape problem, New J. Phys. 21 (2019) 122001.
[22] J.P. Bouchaud, A. Georges, Anomalous diffusion in disordered media: statistical mechanisms, models and physical applications, Phys. Rep. 195 (1990) 127–293.
[23] R. Metzler, J.H. Jeon, A.G. Cherstvy, E. Barkai, Anomalous diffusion models and their properties: non-stationarity, non-ergodicity, and ageing at the centenary of single particle tracking, Phys. Chem. Chem. Phys. 16 (2014) 24128–24164.
[24] V. Zaburdaev, S. Denisov, J. Klafter, Lévy walks, Rev. Mod. Phys. 87 (2015) 483.
[25] M.F. Shlesinger, J. Klafter, On Growth and Form, Springer, 1986.
[26] G.M. Viswanathan, M.G.E. da Luz, E.P. Raposo, H.E. Stanley, The Physics of Foraging, Cambridge University Press, 2011.
[27] N.E. Humphries, H. Weimerskirch, N. Queiroz, E.J. Southall, D.W. Sims, Foraging success of biological Lévy flights recorded in situ, Proc. Natl. Acad. Sci. 109 (2012) 7169–7174.
[28] N.E. Humphries, N. Queiroz, J.R.M. Dyer, N.G. Pade, M.K. Musyl, K.M. Schaefer, D.W. Fuller, J.M. Brunnschweiler, T.K. Doyle, J.D.R. Houghton, G.C. Hays, C.S. Jones, L.R. Noble, V.J. Wearmouth, E.J. Southall, D.W. Sims, Environmental context explains Lévy and Brownian movement patterns of marine predators, Nature 465 (2010) 1066.
[29] V. Fioriti, F. Fratichini, S. Chiesa, C. Moriconi, Lévy foraging in a dynamic environment extending the Lévy search, Int. J. Adv. Robot. Syst. 12 (2015) 98.
[30] D. Brockmann, L. Hufnagel, T. Geisel, The scaling laws of human travel, Nature 439 (2006) 462–465.
[31] B. Gross, Z. Zheng, S. Liu, X. Chen, A. Sela, J. Li, D. Li, S. Havlin, Spatio-temporal propagation of COVID-19 pandemics, arXiv:2003.08382, 2020.
[32] I.M. Sokolov, J. Mai, A. Blumen, Paradoxal diffusion in chemical space for nearest-neighbor walks over polymer chains, Phys. Rev. Lett. 7 (1997) 857.
[33] M.A. Lomholt, T. Ambjörnsson, R. Metzler, Optimal target search on a fast folding polymer chain with volume exchange, Phys. Rev. Lett. 95 (2005) 260603.
[34] M.S. Abe, Lévy walks emerging near a critical point, E-print bioRxiv:2020.01.27.920801, 2020.
[35] M.A. Lomholt, T. Koren, R. Metzler, J. Klafter, Lévy strategies in intermittent search processes are advantageous, Proc. Natl. Acad. Sci. 105 (2008) 11055–11059.
[36] G.M. Viswanathan, V. Afanasyev, S.V. Buldyrev, E.J. Murphy, P.A. Prince, H.E. Stanley, Lévy flight search patterns of wandering albatrosses, Nature 381 (1996) 413–415.

[37] G.M. Viswanathan, S.V. Buldyrev, S. Havlin, M.G.E. da Luz, E.P. Raposo, H.E. Stanley, Optimizing the success of random searches, Nature 401 (1999) 911–914.
[38] E. Estrada, J.C. Delvenne, N. Hatano, J.L. Mateos, R. Metzler, A.P. Riascos, M.T. Schaub, Random multi-Hopper model: super-fast random walks on graphs, J. Complex Netw. 6 (2018) 382–403.
[39] V.V. Palyulin, A.V. Chechkin, R. Metzler, Lévy flights do not always optimize random blind search for sparse targets, Proc. Natl. Acad. Sci. 111 (2014) 2931–2936.
[40] V.V. Palyulin, A.V. Chechkin, R. Metzler, Space-fractional Fokker–Planck equation and optimization of random search processes in the presence of an external bias, J. Stat. Mech. Theory Exp. 2014 (2014) P11031.
[41] A. Reynolds, Liberating Lévy walk research from the shackles of optimal foraging, Phys. Life Rev. 14 (2015) 59–83.
[42] R. Klages, Search for food of birds, fish and insects, Springer, 2018, pp. 49–69.
[43] S. Benhamou, J. Collet, Ultimate failure of the Lévy foraging hypothesis: two-scale searching strategies outperform scale-free ones even when prey are scarce and cryptic, J. Theor. Biol. 387 (2015) 221–227.
[44] T. Koren, M.A. Lomholt, A.V. Chechkin, J. Klafter, R. Metzler, Leapover lengths and first passage time statistics for Lévy flights, Phys. Rev. Lett. 99 (2007) 160602.
[45] A.V. Chechkin, R. Metzler, J. Klafter, V.Y. Gonchar, L.V. Tanatarov, First passage and arrival time densities for Lévy flights and the failure of the method of images, J. Phys. A, Math. Gen. 36 (2003) L537.
[46] V.V. Palyulin, G. Blackburn, M.A. Lomholt, N.W. Watkins, R. Metzler, R. Klages, A.V. Chechkin, First passage and first hitting times of Lévy flights and Lévy walks, New J. Phys. 21 (2019) 103028.
[47] V.V. Palyulin, A.V. Chechkin, R. Klages, R. Metzler, Search reliability and search efficiency of combined Lévy-Brownian motion: long relocations mingled with thorough local exploration, J. Phys. A, Math. Theor. 49 (2016) 394002.
[48] V.V. Palyulin, V.N. Mantsevich, R. Klages, R. Metzler, A.V. Chechkin, Comparison of pure and combined search strategies for single and multiple targets, Eur. Phys. J. B 90 (2017) 170.
[49] D.W. Sims, N.E. Humphries, R.W. Bradford, B.D. Bruce, Lévy flight and Brownian search patterns of a free-ranging predator reflect different prey field characteristics, J. Anim. Ecol. 81 (2012) 432–442.
[50] P.D. Ditlevsen, Observation of alpha-stable noise induced millennial climate changes from an ice-core record, Geophys. Res. Lett. 26 (1999) 1441–1444.
[51] P.D. Ditlevsen, Climate transitions on long timescales, Contemp. Phys. 50 (2009) 511–532.
[52] D.A. Benson, M.M. Meerschaert, J. Revielle, Fractional calculus in hydrologic modeling: a numerical perspective, Adv. Water Resour. 51 (2013) 479–497.
[53] C.E.G. Otiniano, T.R. Sousa, P.N. Rathie, Stable random variables: convolution and reliability, J. Comput. Appl. Math. 242 (2013) 1–11.
[54] F. Mainardi, G. Pagnini, Mellin-Barnes integrals for stable distributions and their convolutions, Fract. Calc. Appl. Anal. 11 (2008) 443–456.
[55] A.V. Chechkin, V.Y. Gonchar, R. Gorenflo, N. Korabel, I.M. Sokolov, Generalized fractional diffusion equations for accelerating subdiffusion and truncated Lévy flights, Phys. Rev. E 78 (2008) 021111.
[56] A.V. Chechkin, R. Gorenflo, I.M. Sokolov, Retarding subdiffusion and accelerating superdiffusion governed by distributed-order fractional diffusion equations, Phys. Rev. E 66 (2002) 046129.
[57] W.L. Wang, E. Barkai, Fractional advection-diffusion-asymmetry equation, Phys. Rev. Lett. 125 (2020) 240606.
[58] M.M. Meerschaert, C. Tadjeran, Finite difference approximations for fractional advection-dispersion flow equations, J. Comput. Appl. Math. 172 (2004) 65–77.
[59] M.M. Meerschaert, C. Tadjeran, Finite difference approximations for two-sided space-fractional partial differential equations, Appl. Numer. Math. 56 (2006) 80–90.
[60] Y. Xu, H. Zhang, Y.G. Li, K. Zhou, Q. Liu, J. Kurths, Solving Fokker-Planck equation using deep learning, Chaos, Interdiscip. J. Nonlinear Sci. 30 (2020) 013133.
[61] M.F. Wehner, W.G. Wolfer, Numerical evaluation of path-integral solutions to Fokker-Planck equations, Phys. Rev. A 27 (1983) 2663–2670.
[62] M.F. Wehner, W.G. Wolfer, Numerical evaluation of path-integral solutions to Fokker-Planck equations. II. Restricted stochastic processes, Phys. Rev. A 28 (1983) 3003–3011.
[63] M.F. Wehner, W.G. Wolfer, Numerical evaluation of path-integral solutions to Fokker-Planck equations. III. Time and functionally dependent coefficients, Phys. Rev. A 35 (1987) 1795–1801.
[64] J.S. Yu, G.Q. Cai, Y.K. Lin, A new path integration procedure based on Gauss-Legendre scheme, Int. J. Non-Linear Mech. 32 (1997) 759–768.
[65] A. Naess, V. Moe, Efficient path integration methods for nonlinear dynamic systems, Probab. Eng. Mech. 15 (2000) 221–231.
[66] A. Naess, V. Moe, Stationary and non-stationary random vibration of oscillators with bilinear hysteresis, Int. J. Non-Linear Mech. 31 (1996) 553–562.
[67] A. Naess, J.M. Johnsen, Response statistics of nonlinear, compliant offshore structures by the path integral solution method, Probab. Eng. Mech. 8 (1993) 91–106.
[68] M. Di Paola, R. Santoro, Path integral solution for non-linear system enforced by Poisson white noise, Probab. Eng. Mech. 23 (2008) 164–169.
[69] A. Di Matteo, M. Di Paola, A. Pirrotta, Path integral solution for nonlinear systems under parametric Poissonian white noise input, Probab. Eng. Mech. 44 (2016) 89–98.
[70] C. Bucher, A. Di Matteo, M. Di Paola, A. Pirrotta, First-passage problem for nonlinear systems under Lévy white noise through path integral method, Nonlinear Dyn. 85 (2016) 1445–1456.
[71] Y. Xu, W.R. Zan, W.T. Jia, J. Kurths, Path integral solutions of the governing equation of SDEs excited by Lévy white noise, J. Comput. Phys. 394 (2019) 41–55.
[72] C. Bucher, M. Di Paola, Efficient solution of the first passage problem by path integration for normal and Poissonian white noise, Probab. Eng. Mech. 41 (2015) 121–128.
[73] G. Volpe, J. Wehr, Effective drifts in dynamical systems with multiplicative noise: a review of recent progress, Rep. Prog. Phys. 79 (2016) 053901.
[74] Y.G. Li, R.X. Mei, Y. Xu, J. Kurths, J.Q. Duan, R. Metzler, Particle dynamics and transport enhancement in a confined channel with position-dependent diffusivity, New J. Phys. 22 (2020) 053016.
[75] D. Schertzer, M. Larcheveque, J. Duan, V.V. Yanovsky, S. Lovejoy, Fractional Fokker-Planck equation for nonlinear stochastic differential equations driven by non-Gaussian Lévy stable noises, J. Math. Phys. 42 (2001) 200–212.
[76] R. Metzler, J. Klafter, The random walk's guide to anomalous diffusion: a fractional dynamics approach, Phys. Rep. 339 (2000) 1–77.
[77] S. Jespersen, R. Metzler, H.C. Fogedby, Lévy flights in external force fields: Langevin and fractional Fokker-Planck equations and their solutions, Phys. Rev. E 59 (1999) 2736.
[78] R. Metzler, E. Barkai, J. Klafter, Deriving fractional Fokker-Planck equations from a generalised master equation, Europhys. Lett. 46 (1999) 431.
[79] S. Nadarajah, S. Chan, The exact distribution of the sum of stable random variables, J. Comput. Appl. Math. 349 (2019) 187–196.
[80] H. Risken, The Fokker-Planck Equation, Springer, 1996.
[81] A. Padash, A.V. Chechkin, B. Dybiec, I. Pavlyukevich, B. Shokri, R. Metzler, First passage properties of asymmetric Lévy flights, J. Phys. A, Math. Theor. 52 (2019) 454004.
[82] A. Padash, A.V. Chechkin, B. Dybiec, M. Magdziarz, B. Shokri, R. Metzler, First passage time moments of asymmetric Lévy flights, J. Phys. A, Math. Theor. 53 (2020) 275002.